Int J Earth Sci (Geol Rundsch) (2017) 106:1429–1451
DOI 10.1007/s00531-016-1437-6

ORIGINAL PAPER

Early Paleozoic subduction initiation volcanism of the Iwatsubodani Formation, Hida Gaien belt, Southwest Japan

Kazuhiro Tsukada[1] · Koshi Yamamoto[2] · Onon Gantumur[2] · Manchuk Nuramkhaan[3]

Received: 31 March 2016 / Accepted: 14 December 2016 / Published online: 24 January 2017

Abstract In placing Japanese tectonics in an Asian context, variation in the Paleozoic geological environment is a significant issue. This paper investigates the geochemistry of the lower Paleozoic basalt formation (Iwatsubodani Formation) in the Hida Gaien belt, Japan, to consider its tectonic setting. This formation includes the following two types of rock in ascending order: basalt A with sub-ophitic texture and basalt B with porphyritic texture. Basalt A has a high and uniform FeO*/MgO ratio, moderate TiO_2, high V, and low Ti/V. The HFSE and REE are nearly the same as those in MORB, and all the data points to basalt A being the "MORB-like fore-arc tholeiitic basalt (FAB)" reported, for example, from the Izu–Bonin–Mariana arc. By contrast, basalt B has a low FeO*/MgO ratio, low TiO_2, and low V and Ti/V. It has an LREE-enriched trend and a distinct negative Nb anomaly in the MORB-normalized multi-element pattern and a moderately high LREE/HREE. All these factors suggest that basalt B is calc-alkaline basalt. It is known that FAB is erupted at the earliest stage of arc formation—namely, subduction initiation—and that boninitic/tholeiitic/calc-alkaline volcanism follows at the supra-subduction zone (SSZ). Thus, the occurrence of basalts A (FAB) and B (calc-alkaline rock) is strong evidence of early Paleozoic arc-formation initiation at an SSZ. Evidence for an early Paleozoic SSZ arc is also recognized from the Oeyama, Hayachine-Miyamori, and Sergeevka ophiolites. Hence, both these ophiolites and the Iwatsubodani Formation probably coexisted in a primitive SSZ system in the early Paleozoic.

Keywords Volcanic arc at SSZ · Fore-arc basalt (FAB) · Hitoegane succession · Fukuji area (Gifu Pref.)

Introduction

The geology of the East Asian continental margin developed through various processes, such as accretion, collision, and strike-slip tectonic movement. Accretion of trench-fill sediments and oceanic plate cover, as well as collision of terranes with strike-slip tectonic movement, created the basic geotectonic framework of southwestern (SW) Japan. Features of the accretionary complexes of this area have been studied, and various tectonic models for their formation presented (e.g., Isozaki et al. 1990; Wakita 1989; Wakita et al. 1992). Although some suggestions have been proposed about the collision process and the role of strike-slip tectonic movement in the evolution of SW Japan, a definitive answer remains a matter to be further researched (e.g., Charvet 2012; Faure and Charvet 1987; Faure et al. 1986; Tashiro 1994; Tazawa 2004; Yamakita and Otoh 2000). The Hida Gaien belt, a major tectonic belt of SW Japan, contains fault-bound blocks of Paleozoic shelf facies rocks. It was formed through Mesozoic strike-slip movements between the Hida and the Sangun–Renge belt (Otoh et al. 2003; Tsukada 2003, Fig. 1). To reveal the Paleozoic geodynamics, understanding the tectonic origin and environmental variation of each block is important. The Hida Gaien belt exposes well-preserved Paleozoic successions and is one of the most important sites for Paleozoic stratigraphy in Japan. Many geologists

✉ Kazuhiro Tsukada
tsukada@num.nagoya-u.ac.jp

[1] The Nagoya University Museum, Nagoya 464-8601, Japan

[2] Graduate School of Environmental Studies, Nagoya University, Nagoya 464-8601, Japan

[3] School of Geology and Mining, Mongolian University of Science and Technology, Ulaanbaatar, Mongolia

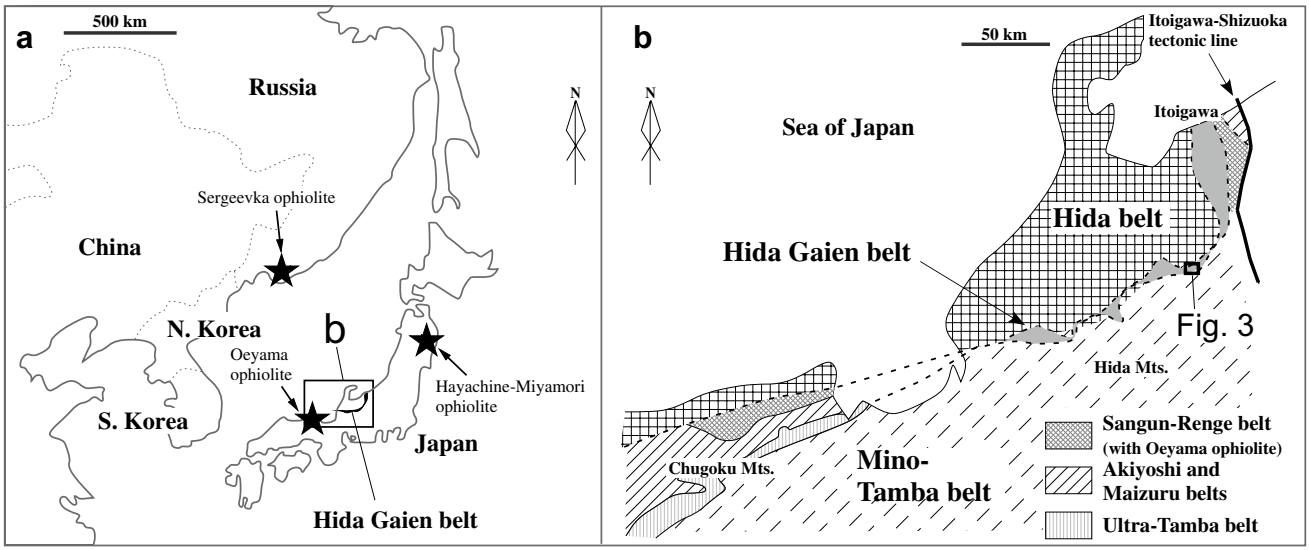

Fig. 1 Index map of the study area

and paleontologists have studied the post-Silurian rocks in this belt (e.g., Adachi 1985; Horikoshi et al. 1987; Igo 1956; Igo and Adachi 1981; Kamei 1952; Kato 1959; Niikawa 1980; Okazaki 1974; Tsukada and Takahashi 2000), but the geological environment in pre-Devonian times has not previously been investigated. The geochemistry of mafic volcanic rocks gives evidence for the tectonic setting of the volcanic activity, because the chemical composition of the present mafic volcanic rocks varies according to their tectonic origins and this provides a basis for geodynamic interpretation. Although little attention has so far been given to the geochemistry of the mafic volcanic rocks of the Iwatsubodani Formation of the Hitoegane succession, which includes the oldest fossil-bearing sedimentary strata in Japan, in the Hida Gaien belt (Fig. 2), it is critical to our understanding of the lower Paleozoic setting in Japan. This paper describes the lithology, stratigraphy, and geochemistry of the Iwatsubodani Formation. Environmental variation of the Hitoegane succession and its regional correlation is also discussed.

Geological framework of the Hida Gaien belt

Southwest Japan is divided into the Inner and Outer zones, and the former is composed of several tectonic belts. These are, from north to south: the Hida, Hida Gaien, Nagato, Sangun–Renge (including Oeyama ophiolite and Sangun–Renge metamorphic rocks), Akiyoshi, Maizuru, Ultra-Tamba, Mino–Tamba, and Ryoke belts (Wakita 1989; Wakita et al. 1992, Fig. 1). The Hida belt consists mainly of Paleozoic metamorphic rocks with Mesozoic cover, while the Ryoke belt has a pre-metamorphic affinity with the Mino–Tamba belt. The Sangun–Renge belt is composed

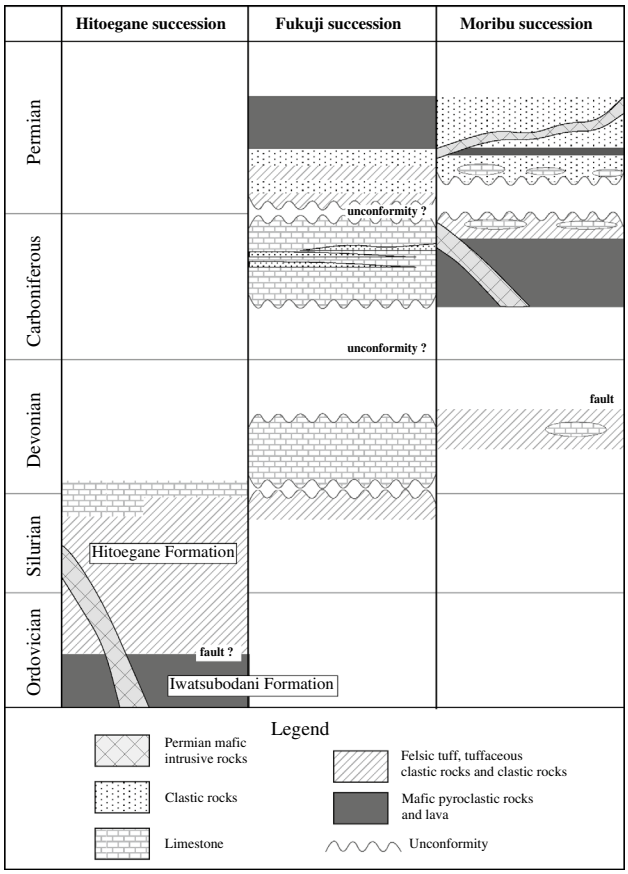

Fig. 2 Schematic stratigraphies of the Hitoegane, Fukuji, and Moribu successions in the Hida Gaien belt (modified from Tsukada 2003)

mainly of lower Paleozoic ophiolite (Oeyama ophiolite), upper Paleozoic blueschist-facies metamorphic rocks (Sangun–Renge metamorphic rocks), and Mesozoic clastic

rocks. The Akiyoshi and Ultra-Tamba belts are Permian to Triassic accretionary complexes, and the Mino–Tamba belt is upper Triassic to lower Cretaceous. The Maizuru belt is an upper Paleozoic island arc entity covered by upper Paleozoic to upper Mesozoic strata. The Nagato belt is considered to be the western extension of the Hida Gaien belt. The Sangun–Renge, Akiyoshi, Maizuru, and Ultra-Tamba belts are widely exposed in the western part of SW Japan (Chugoku Mountains), while these belts are mostly lacking in the eastern part of SW Japan (Hida Mountains), where the Hida Gaien belt is narrowly distributed between the Hida and Mino–Tamba belts (e.g., Tsukada et al. 2004, Fig. 1b).

The Hida Gaien belt, which is a significant tectonic zone in Japan, was formed as a result of Jurassic dextral and Cretaceous sinistral strike-slip movements (Tsukada 2003). It includes several tectonic blocks of Paleozoic rocks which can be divided into the following three types based on their lithostratigraphy: (1) the Hitoegane succession composed of mafic volcanic rocks, and Ordovician to Devonian felsic tuff, tuffaceous clastic rocks, and clastic rocks; (2) the Fukuji succession composed mainly of Silurian felsic tuffaceous clastic rocks and clastic rocks, Devonian limestone, Carboniferous limestone, and Permian felsic tuffaceous clastic rocks, clastic rocks, and mafic pyroclastic rocks; and (3) the Moribu succession composed of Devonian felsic tuff and tuffaceous clastic rocks, Carboniferous mafic pyroclastic rocks, and Permian clastic rocks (Ehiro et al. 2016; Tsukada 2003; Tsukada et al. 2004, Fig. 2).

The mafic volcanic rocks, examined in this paper, are assumed to be in fault contact with the Ordovician rocks in the Hitoegane succession, but the former was originally overlain by the latter as will be discussed later (Tsukada 1997, Fig. 3). The felsic tuff and tuffaceous clastic rocks of the Hitoegane succession, including Ludlowian to Pridolian radiolarians, trilobites, and corals, are correlated with those of the Fukuji succession (Ehiro et al. 2016; Manchuk et al. 2013b and references therein, Fig. 2). The Silurian rocks of the Fukuji succession are largely in fault contact with the surrounding formations, but are partly unconformably overlain by Devonian limestone (Igo 1990). Abundant fossils, such as corals, stromatoporids, brachiopods, trilobites, bivalves, ostracods, conodonts, and others, were recorded from the limestone of early to middle Devonian

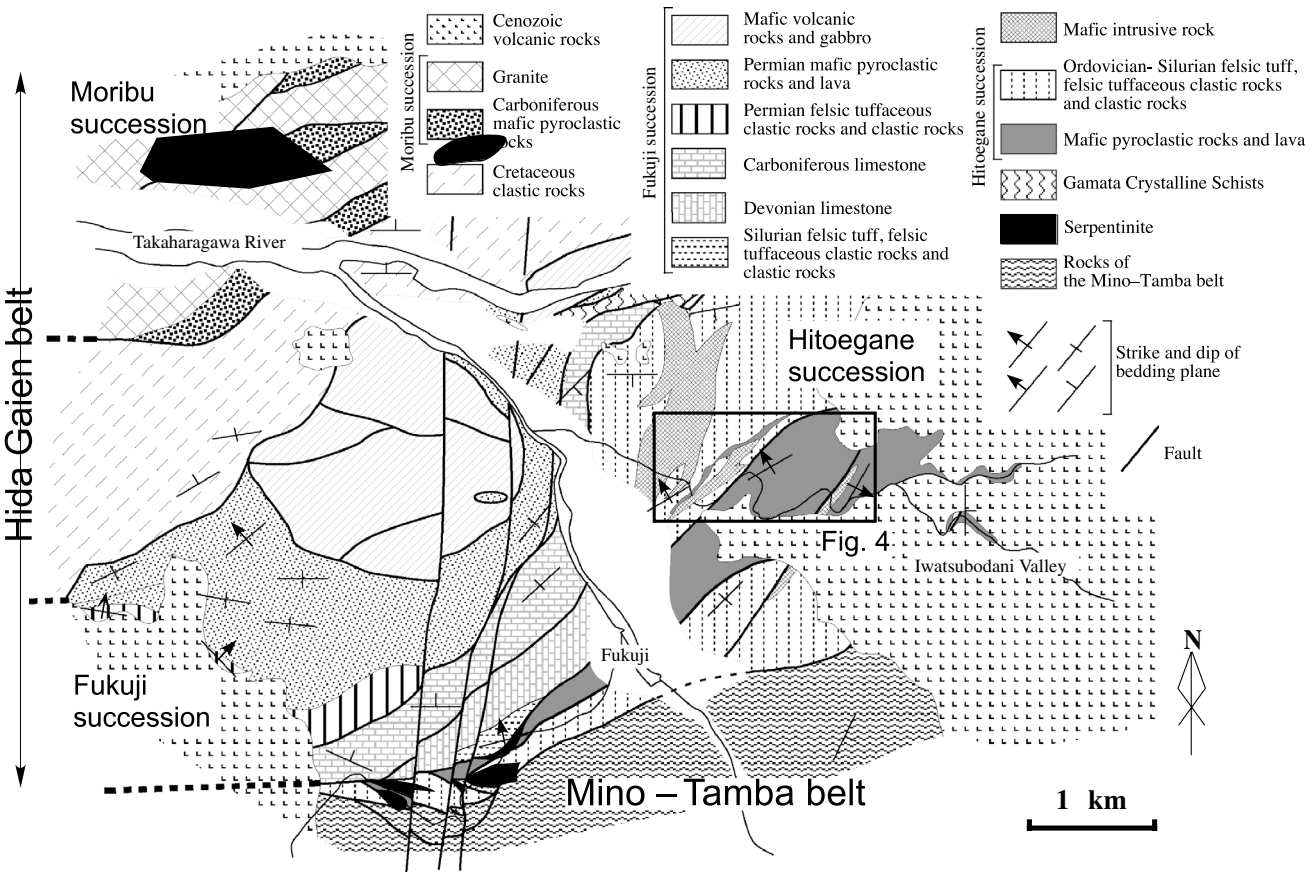

Fig. 3 Simplified geologic map at type locality of the Hida Gaien belt, including Hitoegane, Fukuji, and Moribu successions (modified from Tsukada and Takahashi 2000)

age (Tsukada 2005 and references therein). Investigation of the biostratigraphy of foraminifers and corals from the Carboniferous formation of the Fukuji succession indicates an age of Visean to Gzhelian (e.g., Adachi 1985; Niikawa 1980; Watanabe 1991). This formation intercalates red and gray layers of shale and marl which are considered to have been formed in fresh water lake conditions by deposition of paleosol produced by chemical weathering of limestone (Igo 1960). Smaller foraminifers and corals suggest a tropical to subtropical environment (Adachi 1985; Kato 1959). Devonian and Carboniferous formations are in fault contact each other (Fig. 3). They are, however, likely to have formed a superposing succession (Tsukada and Takahashi 2000; Fig. 2). The lower to upper middle Permian felsic tuffaceous clastic rocks and clastic rocks in this succession are conformably overlain by mafic pyroclastic rock yielding a middle Permian fusulinoidean fauna (Tsukada et al. 1999; Tsukada and Takahashi 2000; Figs. 2, 3).

The Devonian formation in the Moribu succession, which yield crinoids, tabulate corals, and plant fossils (Tazawa et al. 1997, 2000b), are in fault contact with other Paleozoic formations. The upper Visean to upper Kasimovian or Gzhelian (?) mafic pyroclastic rock, which contains corals, ammonoids, foraminifers, brachiopods, and trilobites (Tazawa et al. 2000a and references therein), is unconformably overlain by middle Permian clastic rocks (Horikoshi et al. 1987; Niwa et al. 2004; Fig. 2). The clastic rocks yield brachiopods that form a mixed fauna of Boreal and Tethyan species having a close affinity to the fauna of inner Mongolia (e.g., Horikoshi et al. 1987; Tazawa 1991). A boreal fusulinoidean, genus *Monodiexodina*, was found from this clastic rock formation (Niwa et al. 2004; Tazawa et al. 1993).

Geological description of the Hitoegane succession

The rocks of the Hitoegane succession in and around the Hitoegane area are divided into the following three formations: (1) mafic volcanic rocks of the Iwatsubodani Formation; (2) the Ordovician to Devonian Hitoegane Formation consisting of alternating beds of felsic tuff, tuffaceous clastic rocks, and clastic rocks with minor amounts of limestone lenses; and (3) Gamata Crystalline Schists (Tsukada 1997; Fig. 3). The inference is that the Iwatsubodani Formation is in fault contact with the Hitoegane Formation, but the former was originally overlain by the latter, as discussed later (Tsukada 1997; Fig. 3). The Gamata Crystalline Schists are in fault contact with the Hitoegane Formation. The Iwatsubodani Formation, composed of mafic lava and pyroclastic rock, is narrowly exposed along the Iwatsubodani valley of this area (Figs. 3, 4). The lava exposed in the upper reach of the valley, striking N 30° E and steeply dipping northward, shows eastward-up pillow structure, and the pyroclastic rock has northwestward-up graded bedding striking N 65° E and dipping 90° near the boundary with the Hitoegane Formation (Figs. 3, 4, 5a, b). The pyroclastic rock overlies the lava with an obscure boundary in the upper reaches of the valley. The bedding plane of the pyroclastic rock near the boundary with the lava strikes N 30° E and dips 90° (Fig. 4). The lava is generally fine-grained with a sub-ophitic texture, and the majority of the plagioclase and clinopyroxene crystals are idiomorphic, fresh, and clear (Fig. 5c). The lava partly shows an ophitic texture with idiomorphic to hypidiomorphic laths of plagioclase more than 1 mm in major axis. The lava was partly altered to the extent that some minerals have been replaced by secondary minerals, such as chlorite, muscovite, and opaque minerals. The pyroclastic rock includes abundant angular clasts of basalt, from several millimeters to several tens of centimeters in diameter (Fig. 5d). The clasts are divided into two types by their texture. One type has a porphyritic texture with phenocrysts several millimeters in major axis (Fig. 5e); the other shows a sub-ophitic texture similar to the lava. The majority of the clast is porphyritic basalt, and sub-ophitic basalt is rare. Larger phenocrysts of idiomorphic plagioclase and clinopyroxene are scattered in smaller interstitial patches of plagioclase in the porphyritic basalt (Fig. 5e). The clasts with sub-ophitic texture include abundant small needles of plagioclase less than 0.5 mm in major axis, in a groundmass. The minerals of the groundmass have been partly altered to chlorite, opaque minerals, and others. In this paper, basalts with a sub-ophitic texture are referred to as basalt A and basalt clasts of the pyroclastic rock with porphyritic texture as basalt B.

The Hitoegane Formation consists largely of alternating beds of felsic tuff, tuffaceous clastic rocks, and clastic rocks, well-bedded in beds from several millimeters to 1 m thick. The lower part of this formation includes clasts of mafic volcanic rock, and intercalates mafic pyroclastic rock layers, up to 20 m thick (Tsukada 1997). The clasts of mafic volcanic rock in the Hitoegane Formation are several centimeters in diameter. The pyroclastic rock layers include abundant clinopyroxene crystals and two types of angular mafic volcanic rock clasts which appear in the mafic pyroclastic rock of the Iwatsubodani Formation (Tsukada 1997). The felsic tuff of the lower part of this formation yields Ordovician conodonts, and zircon ages of ca. 436 Ma and ca. 472 Ma (Nakama et al. 2010; Tsukada and Koike 1997; Fig. 4). The beds striking N 55°–60° E and dipping 60° N–90° have northward-up sedimentary structures at the lower part of the Hitoegane Formation. Minor amounts of fossiliferous limestone lenses are included in the upper part of this formation. Silurian trilobites, corals, and radiolarians were reported from the felsic tuff and limestone of the upper part of this formation (Kurihara 2007; Manchuk et al. 2013b and references therein). The mafic intrusive

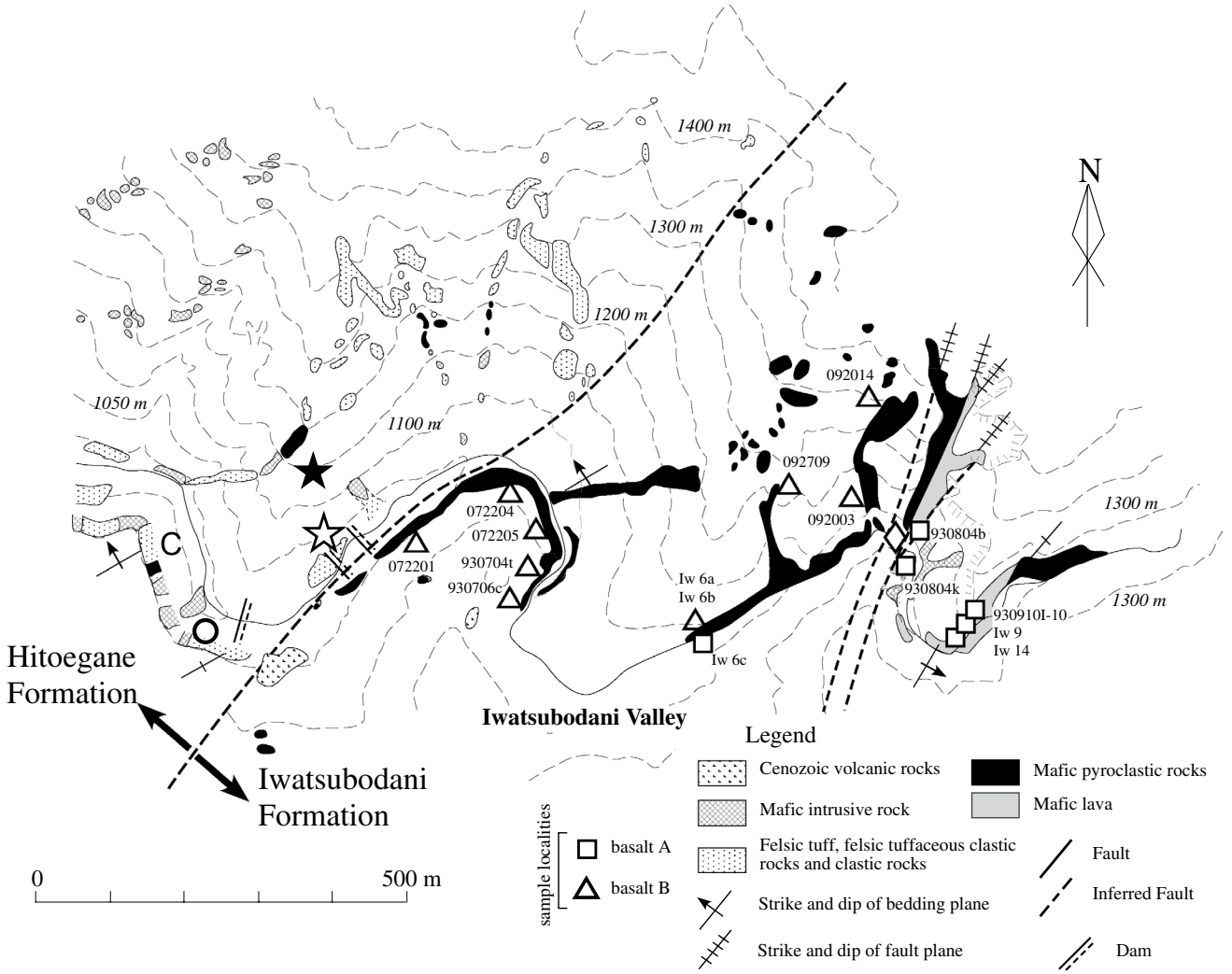

Fig. 4 Route map of the study area showing the sampling localities (modified from Tsukada 1997). C: Ordovician conondont locality (Tsukada and Koike 1997), *white star* ca. 436 Ma zircon locality, *open circle* ca. 472 Ma zircon locality, *black star* ca. 280 Ma zircon locality (Nakama et al. 2010). *White diamond* is the locality of the high-Mg andesite and boninite

rock intrudes into the Iwatsubodani and Hitoegane Formations with an altered porous chilled margin (Tsukada 1997). The rocks in the upper part of Hitoegane Formation generally yield well-preserved radiolarian fossils, but those in the lower part are metamorphosed around the mafic intrusive rock and yield only recrystallized radiolarians which are not identifiable. The intrusive rock is composed mainly of gabbro/diorite, and besides includes dolerite, basalt, and andesite as fine-grained facies. The gabbro/diorite is equigranular, and is composed mainly of idiomorphic clinopyroxene, hornblende, and plagioclase (Figs. 3, 4). In a fine-grained facies, idiomorphic phenocrysts of clinopyroxene, hornblende, and plagioclase, more than 1 mm in length, lie in a groundmass of smaller plagioclase laths, granular clinopyroxene, and interstitial chloritic material (Fig. 5f). Zircon in the gabbro/diorite gives a U-Pb age of ca. 280 Ma (Nakama et al. 2010; Fig. 4). The intermediate dikes, generally less than 3 m wide, intrude into the Iwatsubodani and Hitoegane Formations and the mafic intrusive rock with a clear chilled margin. The dike is composed mainly of idiomorphic plagioclase phenocrysts and a groundmass of small needles of plagioclase. All these are unconformably covered by Cenozoic volcanic rocks (Fig. 3).

Whole-rock chemistry of the basalts of the Iwatsubodani Formation

Sixteen samples from the Iwatsubodani Formation—six of basalt A and ten of basalt B—were analyzed for major and trace elements, including rare-earth elements (REE).

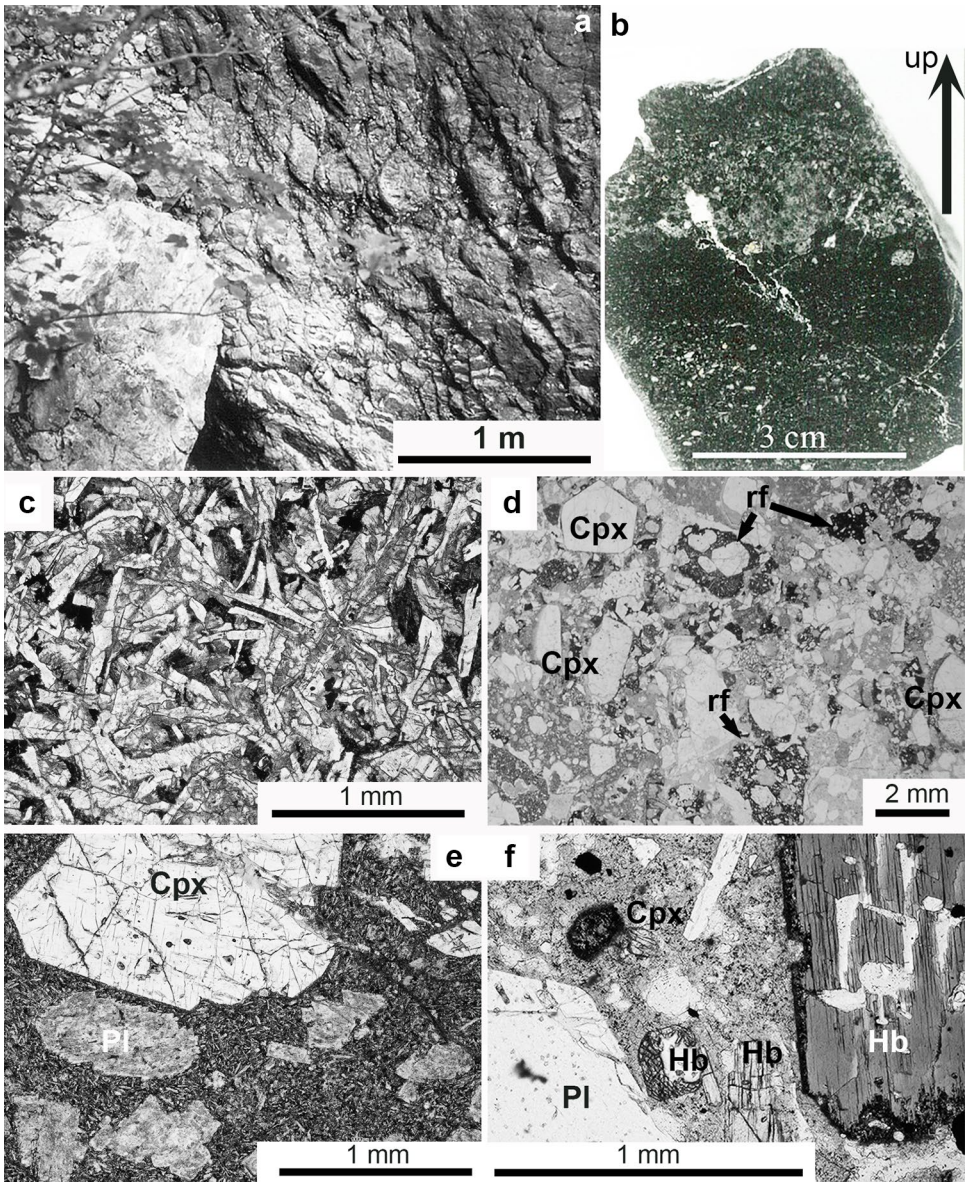

Fig. 5 Photographs of the rocks in the study area. **a** Mafic lava showing pillow structure. It is entirely composed of basalt A. **b** Polished surface of the mafic pyroclastic rock. Clear graded bedding is observed. **c** Photomicograph of the basalt A from the pillow lava showing typical sub-ophitic texture. Plane polarized light. **d** Photomicograph of the mafic pyroclastic rock. It contains only volcanic material, such as volcanic rock fragments and crystals of clinopyroxene and plagioclase. *rf* rock fragment, *Cpx* clinopyroxene. Plane polarized light. **e** Photomicograph of the basalt B from the clast of the pyroclastic rock. Large clinopyroxene (Cpx) and plagioclase (Pl) phenocrysts are embedded in a finer matrix. Plane polarized light. **f** Photomicograph of the mafic intrusive rock with phenocrysts of clinopyroxene (Cpx), plagioclase (Pl), and hornblende (Hb). Plane polarized light

After coarse crushing, veins and altered parts of the samples were excluded using x20 hand loupe. Each analysis sample weighed ca. 200 g. Major element compositions as well as Co, Zn, Ga, and Zr were determined by X-ray fluorescence (XRF; Rigaku Primus II ZSX equipped with Rh X-ray tube, 50 kV, 60 mA), and other trace elements (V, Cr, Ni, Cu, Rb, Sr, Y, Nb, Mo, Pb, Ba, Hf, and Ta) and REE were analyzed by Inductively Coupled Plasma Mass Spectrometry (Quadrupole type ICP-MS; Agilent 7700× with collision cell of He) installed at Nagoya University. In the XRF analysis, glass beads were prepared by fusing mixtures of 1.5 g of powdered sample with 6.0 g of lithium tetraborate. Calibration was carried out using the standard rock samples issued by the Geological Survey of Japan (GSJ) and the composite standards prepared by Yamamoto and Morishita (1997). Analytical precision of major elements was estimated to be <1% for Si and about 3% for other elements, except for TiO_2 and MnO, whose analytical precision is >3% when the measured level is <0.1% (Takebe and Yamamoto 2003) and that for trace elements (Co, Zn, Ga, and Zr) was estimated to be less than 10% (Yamamoto and Morishita 1997). The other trace elements and REE were determined by a method based on that described by Yamamoto et al. (2005) using ICP-MS. About 30 mg of each sample was digested with a mixed solution of HF-$HClO_4$ (2:1 by volume) at 150 °C. After complete evaporation of the acids, 2 ml of 1.7 N-HCl was added to dissolve the cake. The residue was separated by centrifugation at 12,000 rpm with a 2 ml polypropylene tube. After centrifugation, the supernatant was transferred to another 10 ml Teflon beaker. The residue was then fused with HF-$HClO_4$ (2:1 by volume) again at 150 °C. The fused cake

was dissolved with about 2 ml 1.7 N-HCl by mild heating, and the solution was centrifuged at 12,000 rpm. In most cases, no residue was recognized after centrifugation. The HCl solution was evaporated to dryness, and then, the fused cake was re-dissolved in a 2%-HNO_3 solution and determined by ICP-MS. In and Bi were used for tracing ICP sensitivities; the indium and Bi concentrations were mostly the same throughout the analysis. The oxide generation factor (LnO/Ln) was determined for each 20 ppb solution and used for REE analytical data correction. Analytical accuracy was checked by repeated analysis of the standard samples which were prepared from GSJ JB-1a and USGS BCR-1. In the ICP-MS analysis, the correlation coefficients (R values) of each element, calculated for five standard samples, were between 0.9999 and 1.000 and the concentration RSD of the data were mostly less than 3%. The whole-rock compositions of the samples are listed in Table 1, and are displayed on variation diagrams for selected elements against SiO_2 in Fig. 6.

Basalt A (basalt with a sub-ophitic texture)

The SiO_2 concentration is between 48 and 51 wt%, and deviations of each element are <1.3 wt% for major elements, <24 ppm for trace elements except for Sr, and <1.1 ppm for REE. The loss on ignition (LOI) of the samples is less than 2 wt%. The samples are nearly identical to each other in their concentrations of the following elements: TiO_2 ca. 1.3 wt%; Al_2O_3 ca.13 wt%; MnO ca. 0.22 wt%; MgO ca. 6.5 wt%; P_2O_5 ca. 0.11 wt%; Cr ca. 80 ppm; Co ca. 45 ppm; Zn ca. 81 ppm; Ga ca. 16 ppm; and Nb ca. 3.8 ppm (Fig. 6). The samples are slightly increased in Na_2O, K_2O, Sr, and Zr, and reduced in Fe_2O_3*, V, Y, and Hf, with an increase in SiO_2 (Fig. 6). Basalt A has a high FeO*/MgO ratio ranging from 1.9 to 2.5, and is richer than basalt B in TiO_2, Fe_2O_3*, MnO, V, Co, Cu, Zn, Y, Nb, Hf, and Ta (Fig. 6; Table 1). Figure 7a shows a diagram of MORB-normalized multi-element concentrations (called spidergram). The diagram shows a great enrichment in Rb and Ba, and a depletion in P compared with a representative MORB composition, though most of HFSE and HREE form a flat trend which lies along the MORB. Nb and Ta do not exhibit any significant anomaly. The chondrite-normalized REE patterns provide mostly flat characteristics (Fig. 7b).

Basalt B (basalt with porphyritic texture)

The SiO_2 concentration is between 49 and 53 wt%, and deviations of each element are <2.2 wt% for major elements, <40 ppm for trace elements except for Cr and Sr, and <5.2 ppm for REE. The loss on ignition (LOI) of the samples is mostly less than ca. 4 wt%. TiO_2 (ca. 0.60 wt%), Al_2O_3 (ca. 13 wt%), Fe_2O_3 (ca. 11 wt%), MnO (ca. 0.18 wt%), MgO (ca. 8.5 wt%), V (ca. 280 ppm), Co (ca. 37 ppm), Zn (ca. 66 ppm), Ga (ca. 15 ppm), and Y (ca. 12 ppm) show a nearly horizontal flat trend in the variation diagram (Fig. 6). Na_2O, K_2O, P_2O_5, Sr, Zr, Nb, and Ba show an increasing trend, and CaO shows a decreasing trend, correlated with the increase in SiO_2 (Fig. 6). Basalt B has lower FeO*/MgO ratio ranging from 0.8 to 1.9 and has a higher concentration of MgO and Cr than basalt A. This basalt is selectively enriched in Rb, Ba, K, La, Ce, Pr, Sr, and Nd in comparison with the MORB, but depleted in Nb, Ta, P, Zr, Hf, Ti, Y, and HREE (Fig. 7a). The chondrite-normalized REE patterns show a reducing trend—enriched in LREE and depleted in HREE (Fig. 7b).

Mineral chemistry of the basalts of the Iwatsubodani Formation

Clinopyroxene and plagioclase in basalts A and B were analyzed by the Electron Probe Micro Analyzer (EPMA; JEOL JXA-8800) at Nagoya University, using natural and synthetic standard minerals and a conventional procedure. The minerals are generally homogenous in a single grain, and the core of each grain was analyzed. The **c**hemical composition of the clinopyroxene and plagioclase in basalts A and B is shown in Table 2.

Mineral composition of basalt A

Clinopyroxene varies from 53 to 72 in Mg# (=100 Mg/(Fe+Mg)), (average 62). Ca/(Ca+Fe+Mg) is between 0.30 and 0.45, (average 0.38). The TiO_2 content varies in the range between 0.32 and 1.1 wt% (0.74 wt% average), while Cr_2O_3 is less than 0.17 wt%. Al_2O_3 ranges from 1.6 to 4.4 wt%. Plagioclase is $An_{54–67}$ (An = 100Ca/(Ca+Na)).

Mineral composition of basalt B

The Mg# of clinopyroxene in basalt B ranges from 69 to 85 (79 average) and is higher than that of basalt A. Ca/(Ca+Fe+Mg) is between 0.32 and 0.44, (average 0.40). The TiO_2 content, which is from 0.29 to 0.64 wt% (0.39 wt% average), is generally lower than that of basalt A, and shows a negative correlation with Mg#. Al_2O_3 content varies from 2.2 to 2.8 wt% and Cr_2O_3 is less than 0.35 wt%.

Discussion

Age of the Iwatsubodani Formation

Nakama et al. (2010) reported a U-Pb age of ca. 280 Ma from zircons in a gabbro/diorite of the mafic intrusive rock

Table 1 Whole-rock chemical composition of the basalts A and B displayed to three significant digits, except for Co, Zn, Ga, and Zr

Occurence sample no.	Basalt A						Basalt B									
	Lava	Lava	Lava	Clast	Lava	Lava	Clast	Clast	Clast	Clast	Clast	Clast	Clast	Clast	Clast	Clast
	930804b	930804k	930910I-10	Iw 6c	Iw 9	IW 14	092003	092014	092709	Iw 6a	Iw 6b	930706c	930704t	072201	072204	072205
Major element oxides (wt%)																
SiO_2	48.8	50.8	49.5	48.1	49.5	48.7	50.4	50.7	51.6	49.6	49.0	50.7	52.9	49.2	49.8	49.7
TiO_2	1.30	1.33	1.21	1.40	1.30	1.41	0.627	0.705	0.697	0.661	0.633	0.529	0.737	0.509	0.462	0.423
Al_2O_3	12.8	12.6	13.8	12.6	12.0	12.4	17.8	12.7	16.1	12.1	12.2	10.8	14.6	12.3	14.1	16.4
Fe_2O_3[a]	16.1	14.6	14.0	16.8	16.3	17.8	10.5	11.2	8.97	12.7	12.8	10.5	10.9	9.43	10.8	10.4
MnO	0.239	0.215	0.196	0.224	0.231	0.246	0.161	0.188	0.136	0.193	0.194	0.202	0.177	0.192	0.177	0.168
MgO	7.14	6.26	6.75	6.28	5.87	6.44	4.97	9.48	8.84	10.1	9.33	11.6	6.77	8.83	7.26	7.37
CaO	9.86	8.93	10.6	10.0	10.1	8.66	9.73	9.97	6.97	9.64	11.1	11.2	6.54	14.1	12.74	9.59
Na_2O	2.45	3.89	2.53	3.21	3.59	3.44	4.41	3.39	4.15	3.47	3.12	2.78	5.01	3.28	2.62	3.96
K_2O	0.164	0.213	0.309	0.062	0.147	0.194	0.143	0.398	0.561	0.146	0.106	0.363	1.20	0.617	0.089	0.659
P_2O_5	0.109	0.113	0.103	0.124	0.125	0.124	0.137	0.155	0.171	0.213	0.206	0.127	0.208	0.143	0.117	0.0630
Total	99.0	99.0	98.9	98.8	99.1	99.4	98.9	98.8	98.2	98.8	98.8	98.9	99.0	98.5	98.2	98.7
LOI	1.48	1.81	1.99	1.78	1.20	1.29	3.39	2.64	4.47	2.38	1.75	1.96	1.94	5.36	2.39	3.60
Trace elements (ppm)																
V	412	397	364	430	370	456	295	390	264	206	259	264	281	250	273	324
Cr	63.2	87.0	118	63.9	64.2	81.8	45.0	266	208	301	319	238	85.3	187	201	80.2
Co[b]	46	45	45	45	44	45	32	40	32	46	39	43	31	39	32	31
Ni	63.3	112	130	90.6	97.3	127	52.7	74.6	80.4	69.8	108	149	55.2	119	87.8	36.7
Cu	122	124	171	166	113	164	166	173	62.1	88.0	109	63.4	124	96.8	82.3	48.6
Zn[b]	87	81	74	83	75	85	68	80	69	77	68	57	62	53	62	60
Ga[b]	17	15	16	16	16	16	17	15	19	13	14	14	14	14	16	17
Rb	7.25	6.57	9.35	4.76	427	6.88	7.74	6.99	9.74	5.50	5.37	7.18	9.93	13.7	2.03	15.7
Sr	173	159	201	77	145	106	223	325	363	140	153	172	357	219	180	234
Y	24.6	24.0	23.4	27.9	25.6	29.1	13.1	12.3	13.4	12.5	12.8	9.34	13.9	10.6	10.4	9.2
Zr[b]	47	62	51	46	50	45	30	53	91	41	40	37	70	40	32	29
Nb	3.19	3.91	3.59	3.89	3.94	4.55	1.07	1.68	2.14	1.21	1.37	1.45	2.58	1.55	1.71	0.81
Mo	b.d.l.	2.78	1.85	3.26	2.78	3.29	3.44	2.87	2.07	3.28	8.46	1.80	b.d.l.	b.d.l.	b.d.l.	1.91
Pb	2.90	b.d.l.	1.80	1.59	b.d.l.	b.d.l.	2.46	3.23	2.30	b.d.l.	b.d.l.	1.46	3.32	2.92	3.11	1.98
Ba	25.0	23.0	46.0	13.0	16.5	19.3	30.6	192	139	10.9	13.2	55.9	163	72.0	12.7	59.9
Hf	1.95	1.86	1.59	2.14	2.06	2.27	1.12	1.57	1.69	1.74	1.64	1.27	1.74	1.15	1.12	0.647
Ta	0.240	0.257	0.267	0.300	0.270	0.329	0.090	0.121	0.0712	0.0866	0.105	0.107	0.202	0.129	0.319	0.0718
Rare-earth elements (ppm)																
La	4.12	4.06	3.81	5.05	4.35	4.91	5.57	5.57	7.38	4.88	5.24	3.54	8.28	6.12	4.98	1.81

Table 1 (continued)

Occurence sample no.	Basalt A						Basalt B									
	Lava	Lava	Lava	Clast	Lava	Lava	Clast	Clast	Clast	Clast	Clast	Clast	Clast	Clast	Clast	Clast
	930804b	930804k	930910I-10	Iw 6c	Iw 9	IW 14	092003	092014	092709	Iw 6a	Iw 6b	930706c	930704t	072201	072204	072205
Ce	10.9	11.0	10.1	13.1	11.2	12.7	12.2	14.3	18.7	16.0	17.1	10.1	22.6	14.0	11.7	4.69
Pr	1.66	1.66	1.54	1.97	1.66	1.89	1.77	2.26	2.78	2.63	2.78	1.68	3.30	2.06	1.70	0.753
Nd	8.54	8.75	8.03	10.2	8.58	10.1	8.36	11.6	13.8	13.9	14.1	8.59	16.0	9.92	8.10	3.92
Sm	2.69	2.83	2.62	3.22	2.82	3.14	2.23	3.01	3.49	3.71	3.83	2.35	3.80	2.51	2.04	1.20
Eu	1.08	1.11	1.05	1.29	1.12	1.44	0.960	1.05	1.15	1.09	1.19	0.725	1.06	0.944	0.687	0.458
Gd	3.82	3.87	3.60	4.45	3.78	4.32	2.41	2.90	3.30	3.47	3.46	2.35	3.51	2.47	2.06	1.48
Tb	0.664	0.672	0.629	0.771	0.676	0.744	0.375	0.414	0.467	0.464	0.456	0.339	0.479	0.336	0.304	0.240
Dy	4.49	4.64	4.26	5.35	4.56	5.08	2.61	2.58	2.84	2.63	2.71	2.07	2.98	2.21	1.94	1.78
Ho	0.958	0.996	0.927	1.14	0.975	1.11	0.546	0.519	0.562	0.502	0.526	0.427	0.576	0.436	0.398	0.376
Er	2.85	2.92	2.71	3.41	2.91	3.25	1.65	1.41	1.55	1.38	1.46	1.16	1.62	1.25	1.21	1.15
Tm	0.413	0.415	0.389	0.477	0.426	0.470	0.243	0.198	0.209	0.189	0.200	0.155	0.224	0.173	0.170	0.173
Yb	2.66	2.86	2.52	3.16	2.69	3.00	1.54	1.25	1.29	1.22	1.26	1.03	1.43	1.15	1.14	1.13
Lu	0.396	0.393	0.367	0.450	0.397	0.432	0.232	0.180	0.178	0.172	0.188	0.154	0.205	0.152	0.170	0.182

[a] Fe_2O_3, total ion as Fe_2O_3

[b] Trace elements analyzed by XRF

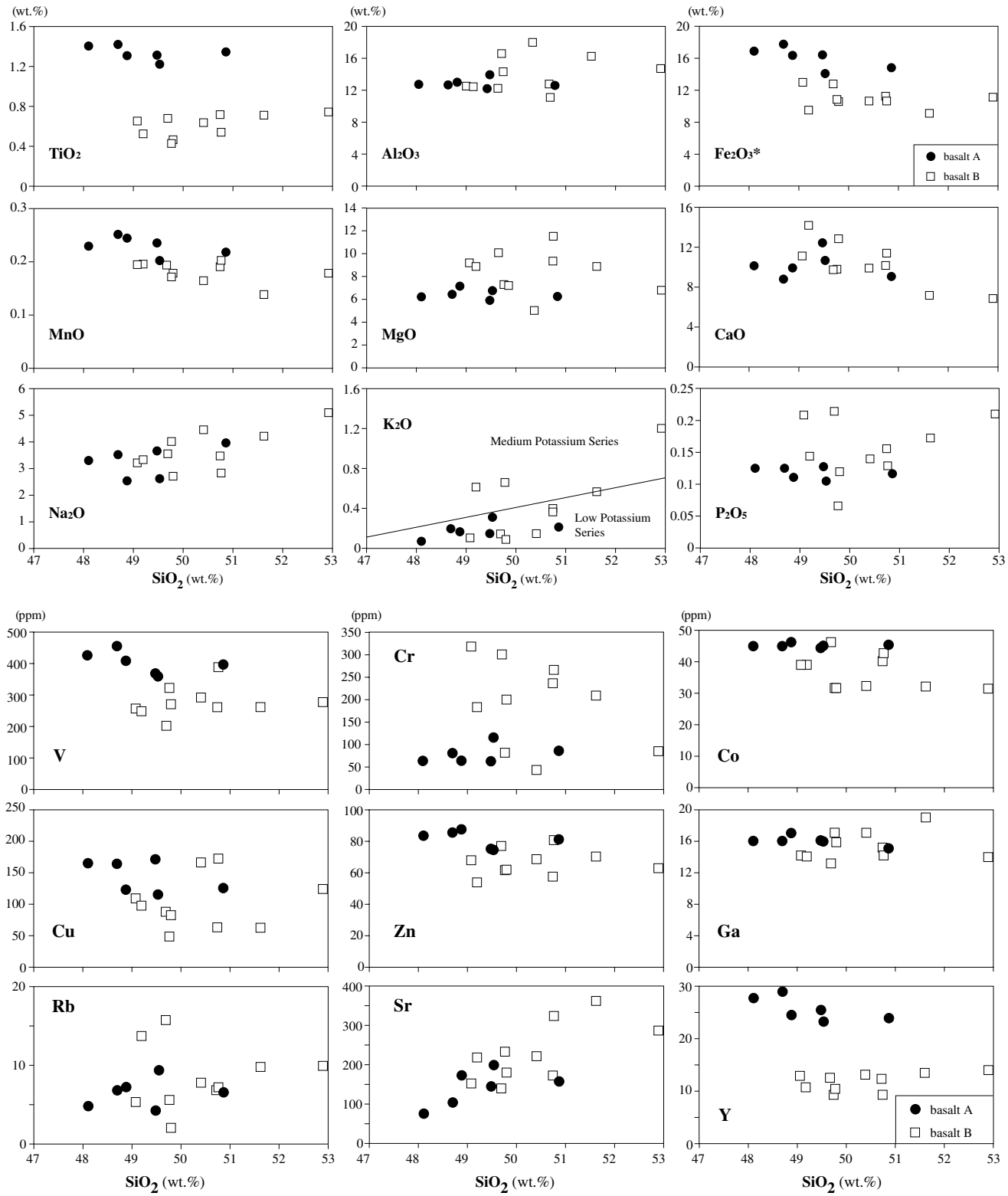

Fig. 6 Variation diagrams of selected elements

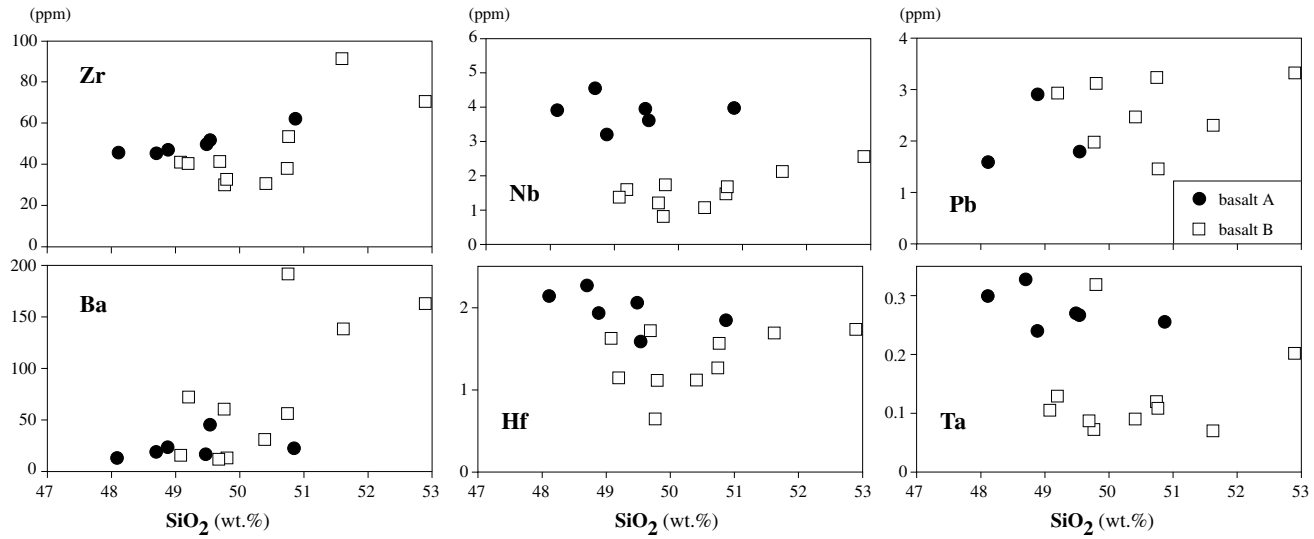

Fig. 6 (continued)

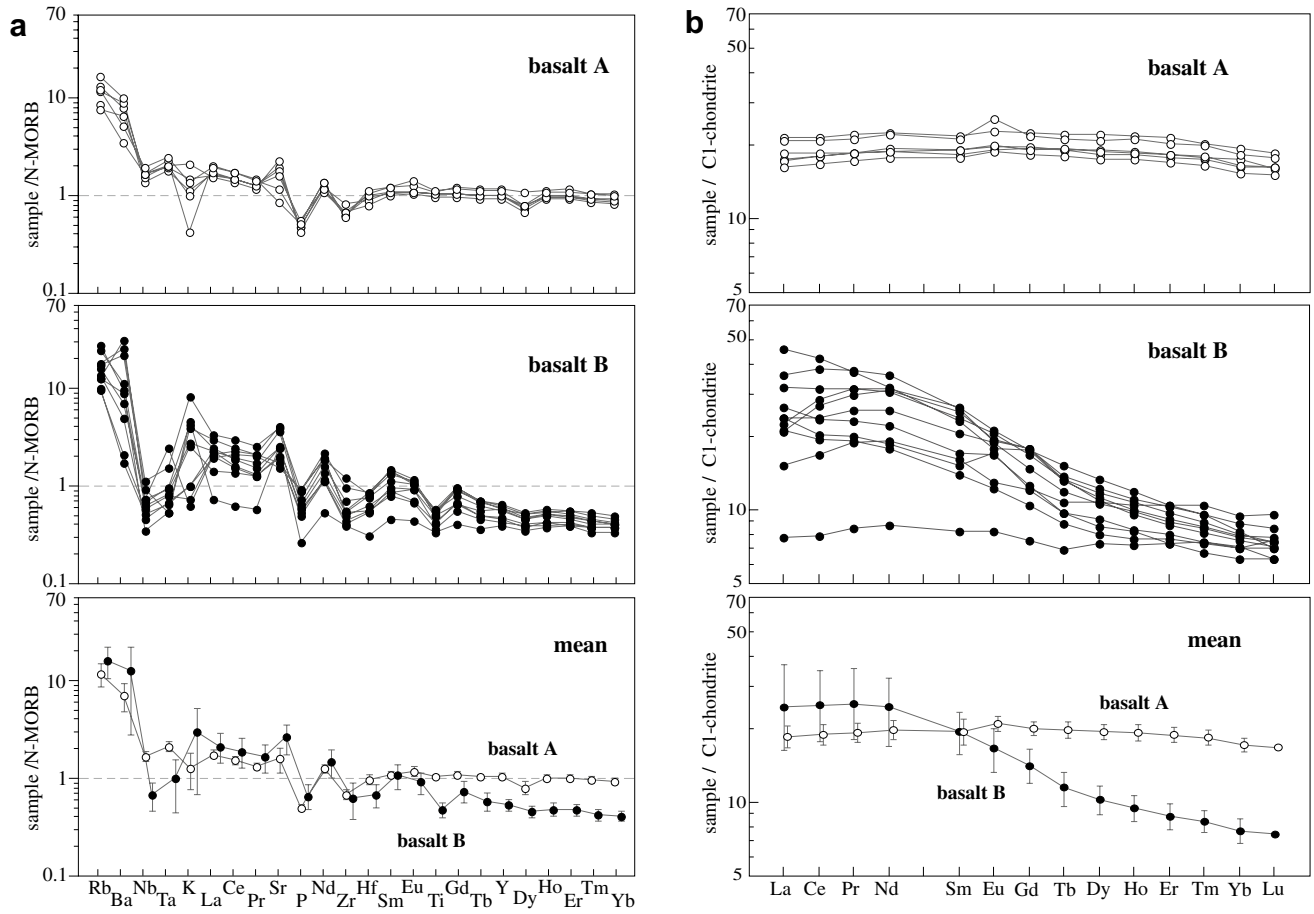

Fig. 7 **a** MORB-normalized multi-element concentration diagrams of the examined samples. The order of elements is after Pearce and Stern (2006). Normalizing MORB composition by Sun and McDonough (1989) is used. **b** Chondrite-normalized REE patterns of the examined samples. Normalizing chondrite concentrations are after Anders and Grevesse (1989) and Yamamoto et al. (2005)

Table 2 Chemical composition of plagioclase and clinopyroxene

Occurrence mineral	Basalt A													
	Lava													
	Pl	Pl	Pl	Pl	Pl	Pl	Pl	Cpx	Cpx	Cpx	Cpx	Cpx	Cpx	Cpx
SiO_2	53.56	54.87	52.87	53.45	51.41	52.53	53.34	50.45	49.75	50.04	50.82	49.38	49.06	50.55
TiO_2	b.d.l	b.d.l	b.d.l	b.d.l	b.d.l	b.d.l	b.d.l	0.47	0.70	0.75	0.44	1.04	0.95	0.66
Al_2O_3	28.13	27.70	28.35	27.85	29.56	28.88	28.24	3.48	2.37	1.79	1.88	2.73	2.71	2.80
Cr_2O_3	b.d.l	b.d.l	b.d.l	b.d.l	b.d.l	b.d.l	b.d.l	0.10	b.d.l	b.d.l	b.d.l	b.d.l	b.d.l	b.d.l
FeO[a]	1.11	1.04	1.00	1.20	0.85	1.05	1.13	12.37	15.84	19.84	14.07	17.56	16.36	10.99
MnO	b.d.l	b.d.l	b.d.l	b.d.l	b.d.l	b.d.l	b.d.l	0.32	0.40	0.48	0.36	0.41	0.31	0.26
MgO	0.14	0.16	0.17	0.16	0.25	0.17	0.17	16.79	13.52	12.61	15.02	12.49	11.82	14.68
CaO	11.87	11.27	12.11	12.00	13.85	12.65	12.08	14.94	16.62	14.08	15.75	16.21	18.38	18.79
Na_2O	4.79	5.32	4.73	4.79	3.71	4.23	4.62	0.22	0.24	0.16	0.22	0.24	0.31	0.20
Total	99.60	100.35	99.23	99.45	99.62	99.50	99.58	99.15	99.44	99.75	98.56	100.05	99.91	98.94
O=	8	8	8	8	8	8	8	6	6	6	6	6	6	6
Si	2.435	2.468	2.411	2.434	2.348	2.397	2.427	1.895	1.907	1.932	1.940	1.894	1.888	1.911
Ti	–	–	–	–	–	–	–	0.013	0.020	0.022	0.013	0.030	0.028	0.019
Al	1.507	1.468	1.523	1.494	1.591	1.553	1.514	0.154	0.107	0.082	0.085	0.124	0.123	0.125
Cr	–	–	–	–	–	–	–	0.003	–	–	–	–	–	–
Fe^{2+}	0042	0.039	0.038	0.046	0.033	0.040	0.043	0.388	0.508	0.640	0.449	0.563	0.526	0.347
Mn	–	–	–	–	–	–	–	0.010	0.013	0.016	0.012	0.013	0.010	0.008
Mg	0.010	0.011	0.012	0.011	0.017	0.012	0.012	0.940	0.772	0.726	0.855	0.714	0.678	0.827
Ca	0.578	0.543	0.591	0.585	0.678	0.618	0.589	0.601	0.683	0.582	0.644	0.666	0.758	0.761
Na	0.422	0.464	0.418	0.423	0.328	0.374	0.407	0.016	0.018	0.012	0.017	0.017	0.023	0.015
Total	4.994	4.993	4.993	4.993	4.994	4.994	4.993	4.021	4.028	4.011	4.013	4.022	4.034	4.014
Pl An	57.79	53.94	58.58	58.06	67.38	62.28	59.12	–	–	–	–	–	–	–
Mg#	–	–	–	–	–	–	–	70.76	60.34	53.12	65.55	55.91	56.30	70.43

Occurrence mineral	Basalt A							Basalt B							
	Lava							Clast							
	Cpx	Cpx	Cpx	Cpx	Cpx	Cpx	Cpx	Cpx	Cpx	Cpx	Cpx	Cpx	Cpx	Cpx	Cpx
SiO_2	48.02	49.09	48.81	49.19	49.44	50.34	49.93	50.68	52.74	52.75	51.41	52.81	52.79	53.38	52.40
TiO_2	0.32	1.12	0.96	0.59	0.81	0.82	0.20	0.64	0.43	0.29	0.43	0.30	0.38	0.30	0.33
Al_2O_3	4.07	4.80	4.24	2.68	4.43	3.85	1.63	2.76	2.21	2.53	2.85	2.31	2.27	2.24	2.25
Cr_2O_3	0.17	0.16	0.12	b.d.l	0.11	0.08	b.d.l	b.d.l	0.10	0.35	b.d.l	0.22	0.12	0.21	0.15
FeO[a]	14.58	11.70	12.57	14.01	17.15	10.92	14.81	12.85	9.27	6.58	9.60	7.60	8.50	6.61	9.43
MnO	0.46	0.36	0.35	0.50	0.32	0.20	0.48	0.30	0.27	0.18	0.33	0.21	0.26	0.19	0.31
MgO	13.40	14.96	13.36	12.49	12.56	15.40	9.93	16.29	16.35	16.42	15.23	16.84	16.11	16.29	16.21
CaO	15.53	16.81	18.25	17.87	13.06	17.81	21.14	15.20	19.25	21.27	19.81	19.65	19.82	21.14	19.30
Na_2O	0.14	0.23	0.23	0.15	0.38	0.23	0.18	0.17	0.33	0.29	0.32	0.26	0.27	0.28	0.33
Total	96.67	99.23	98.87	97.47	98.25	99.58	98.30	98.89	100.85	100.29	99.96	99.96	100.40	100.42	100.56
O=	6	6	6	6	6	6	6	6	6	6	6	6	6	6	6
Si	1.880	1.850	1.863	1.915	1.904	1.883	1.952	1.913	1.936	1.930	1.915	1.940	1.941	1.949	1.932
Ti	0.009	0.032	0.028	0.017	0.023	0.023	0.006	0.018	0.012	0.008	0.012	0.008	0.010	0.008	0.009
Al	0.188	0.213	0.191	0.123	0.201	0.170	0.075	0.123	0.096	0.109	0.125	0.100	0.098	0.096	0.098
Cr	0.005	0.005	0.004	–	0.003	0.002	–	–	0.003	0.010	–	0.007	0.004	0.006	0.004
Fe^{2+}	0.477	0.369	0.401	0.456	0.552	0.342	0.484	0.406	0.238	0.161	0.233	0.209	0.239	0.197	0.230
Mn	0.015	0.011	0.011	0.016	0.010	0.006	0.016	0.010	0.008	0.006	0.010	0.006	0.008	0.006	0.010
Mg	0.782	0.841	0.760	0.725	0.721	0.859	0.579	0.916	0.894	0.896	0.846	0.922	0.883	0.887	0.891
Ca	0.651	0.679	0.746	0.745	0.539	0.714	0.885	0.615	0.757	0.834	0.791	0.773	0.781	0.827	0.762
Na	0.011	0.017	0.017	0.011	0.028	0.017	0.014	0.006	0.012	0.010	0.011	0.009	0.010	0.010	0.012

Table 2 (continued)

Occurrence mineral	Basalt A							Basalt B							
	Lava							Clast							
	Cpx	Cpx	Cpx	Cpx	Cpx	Cpx	Cpx	Cpx	Cpx	Cpx	Cpx	Cpx	Cpx	Cpx	Cpx
Total	4.018	4.017	4.020	4.010	3.981	4.016	4.011	4.006	3.956	3.963	3.943	3.974	3.975	3.987	3.947
Pl An	–	–	–	–	–	–	–	–	–	–	–	–	–	–	–
Mg#	62.10	69.51	65.46	61.39	56.64	71.54	54.46	69.32	78.98	84.73	78.40	81.54	78.68	81.79	79.48

Pl plagioclase, *Cpx* clinopyroxene, *An* anorthite

Mg# = 100 × Mg/(Mg+Fe)

[a]FeO is total ion as FeO

("dolerite/gabbro" in their paper) along the Iwatsubodani Valley (Fig. 4) and, therefore, assigned a Permian age to the Iwatsubidani Formation. However, the dated gabbro/diorite locality is within the distribution area of the rocks of the Hitoegane Formation (Fig. 4), and therefore, the age of the gabbro/diorite does not necessarily indicate the age of volcanic activity of the Iwatsubodani Formation, because the relationship between the dated rock and the mafic volcanic rocks of the Iwatsubidani Formation is uncertain. In addition, the fine-grained facies of the "gabbro/diorite" include idiomorphic phenocrysts of hornblende and plagioclase more than 1 mm in major axis, so it is quite different from the Iwatsubodani basalt in both texture and mineral composition (Fig. 5c, e, f). Thus, the suggestion that the gabbro/diorite and the rocks of the Iwatsubodani Formation were formed by a single magmatism is not backed up by the evidence (Tsukada 1997). Hence, it is not appropriate to link the age of the Iwatsubodani Formation to that of the gabbro/diorite from the stratigraphic or the petrographic viewpoint. Tsukada (1997) suggested that the Iwatsubodani Formation was primarily overlain by the Hitoegane Formation based on the following facts: (1) the lower part of the Hitoegane Formation includes many mafic volcanic clasts; (2) the Hitoegane Formation intercalates mafic pyroclastic rock layers, including clasts of both A and B basalts; (3) the sedimentary structures of both the Iwatsubodani and Hitoegane Formations indicate northwestward-up around their boundary; and (4) the strike and dip of the bedding planes of the Iwatsubodani and Hitoegane Formations are mostly the same around their boundary (Fig. 4). Llanvirnian to Caradocian conodonts, *Periodon aculeatus*, were obtained from the lower part of the Hitoegane Formation (Tsukada and Koike 1997), and Nakama et al. (2010) reported zircon ages of ca. 472 Ma, assigned from the latest Cambrian/earliest Ordovician to Caradocian (International Commission on Stratigraphy ed. 2015), from felsic tuff of the lowest horizon of this formation (Fig. 4). These lines of evidence all point to the age of the Iwatsubodani Formation being earlier than late Ordovician.

Tectonic setting of the Iwatsubodani Formation

The geochemistry of basalt gives evidence for the tectonic setting of the volcanic activity that formed it because the chemical composition of basalt varies according to its origins, and many discrimination diagrams of basaltic rocks have been proposed (e.g., Pearce 1982). In this section, discrimination diagrams are used to discuss the tectonic setting and magma type of the basalts of the Iwatsubodani Formation.

Na, K, Ca, Rb, Ba, and Sr are known to be highly mobile through secondary processes. Discrimination of the analyzed basalts is mainly based on the diagrams using relatively fluid-immobile elements, such as Ti, Fe, Mg, P, V, Y, Zr, Nb, and REE.

Tectonic setting of basalt A

Basalt is generally formed at a mid-oceanic ridge, a volcanic arc, or in an intra-oceanic/-continental plate (i.e., within-plate). It can be divided into alkaline and non-alkaline basalts, the latter further subdivided into tholeiitic and calc-alkaline basalts by their magma source variations and resulting chemical compositions (e.g., Miyashiro and Kushiro 1975; Pearce 1982). The HFSE vs. La/Yb diagrams of basalt A (Nakamura et al. 2000) suggest that the samples are non-alkaline basalt (Fig. 8). In some diagrams with relatively immobile elements, such as Ti, P, Y, Zr, and Nb, the data are plotted in the field of MORB or volcanic arc basalt (VAB) (e.g., Mullen 1983; Pearce 1982, 1983; Pearce and Cann 1973, Fig. 9). Both the Zr/Y vs. Zr diagram (Pearce 1983) and the Ti vs. Zr diagram (Pearce 1982) indicate MORB or VAB (Fig. 9a, b). In addition, the data cluster in the field of low-potassium tholeiite (LPT) of volcanic arc in the Zr–Ti/100–3Y diagram (Pearce and Cann 1973; Fig. 9c). The LPT and CAB in this diagram do not necessarily mean that the rock originated from magmas of tholeiite and calc-alkaline series, because the results

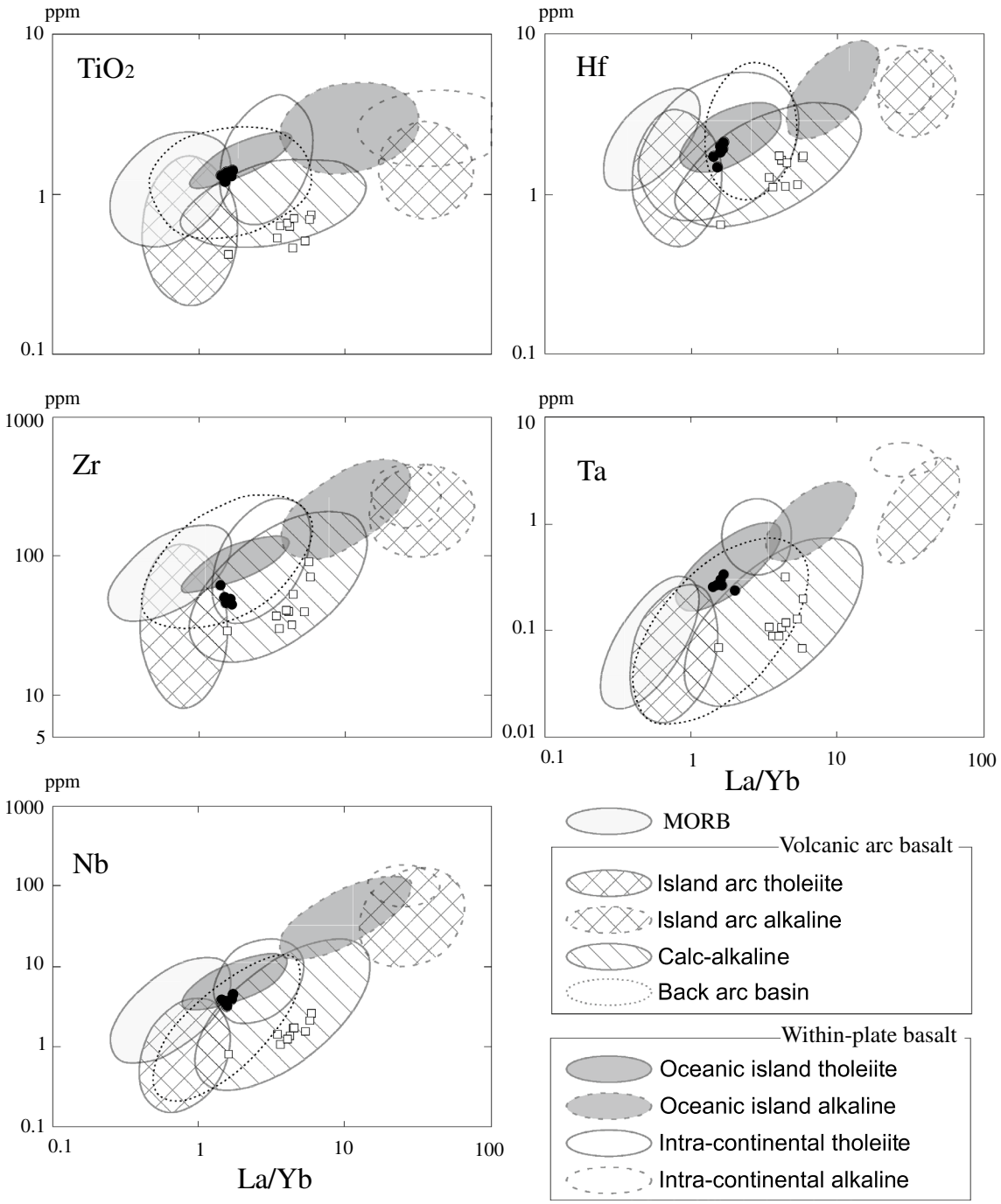

Fig. 8 HFSE vs. La/Yb diagrams (Nakamura et al. 2000)

are very similar to those from the magmas of low- and medium-potassium series basalt in volcanic arcs (e.g., Ujike 1989). Taking all these lines of evidence together, it is reasonable to conclude that the rocks were formed in low-potassium series magma at a volcanic arc. In the SiO_2 vs. FeO*/MgO diagram, SiO_2 of basalt A is almost kept constant regardless of their FeO*/MgO ratio, suggesting tholeiitic affinity of the magma (Miyashiro 1974; Fig. 9d), and the $MnO–TiO_2–P_2O_5$ diagram (Mullen 1983) also indicates their island arc tholeiite (IAT) affinity (Fig. 9e).

One of the important geochemical indicators in volcanic arc basalts is depletion in HFSE (esp. Nb and Ta) compared with LILE and LREE, a feature that is not observed in MORB (e.g., Gill 1981; Pearce et al. 2005). The spidergram for basalt A samples shows an enrichment of LILE

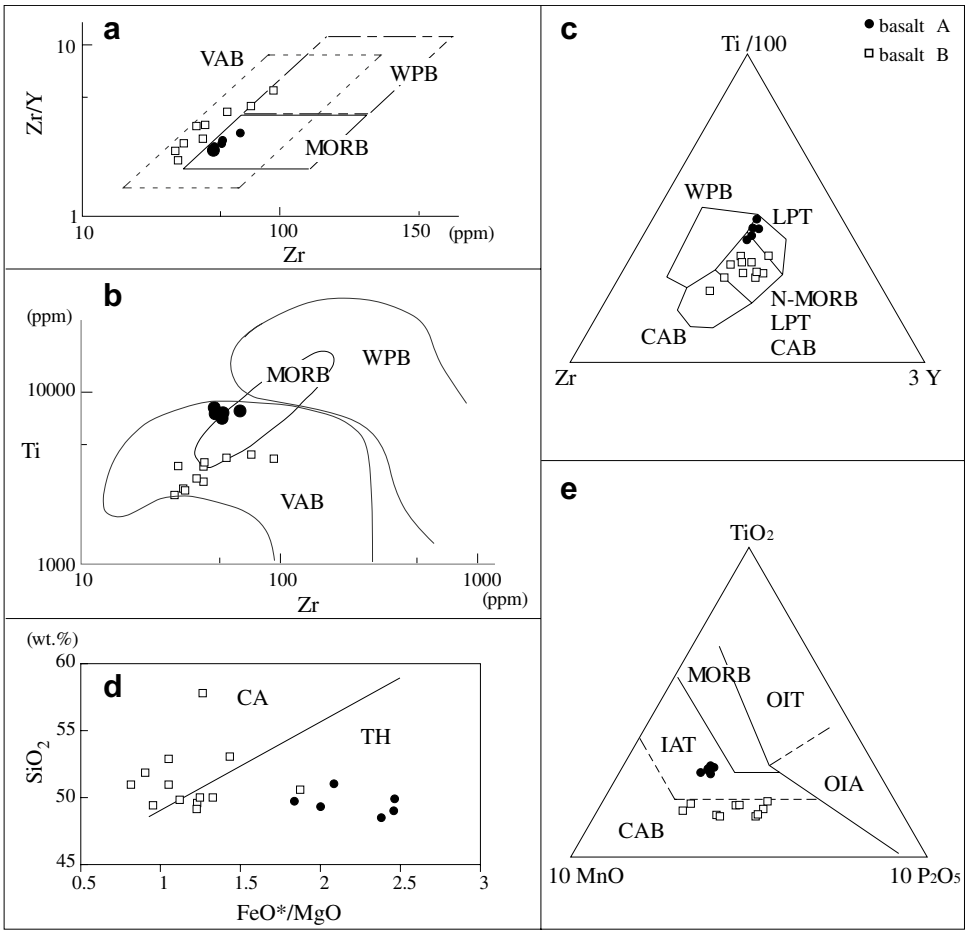

Fig. 9 Discrimination diagrams of **a** Zr/Y vs. Zr (Pearce 1982), **b** Ti vs. Zr (Pearce 1983), **c** Zr–Ti/100–3Y (Pearce and Cann 1973), **d** SiO_2 vs. FeO*/MgO (Miyashiro 1974), and **e** MnO–TiO_2–P_2O_5 (Mullen 1983)

in comparison with HFSE, similar to volcanic arc basalt. However, the HFSE and HREE of basalt A show a flat trend as seen in the MORB, and there is no negative Nb and Ta anomaly (Fig. 7a).

In chondrite-normalized REE patterns, MORB and IAT generally show a horizontal flat line with a comparatively wide range in LREE, while the CAB shows a gradual HREE depletion (Nakamura et al. 2000 and references therein). The present samples show horizontal flat REE patterns which are similar to MORB or IAT (Fig. 7b). Ti vs. (Ca + Na) and (Ti + Cr) vs. Ca diagrams for clinopyroxene phenocryst (Leterrier et al. 1982) indicate "non-orogenic tholeiite" of which the most important type is MORB (Fig. 10a, b). It has long been known that the composition of major constituent minerals in basaltic rocks crystallized from MORB magmas is clearly different from the composition of those crystallized from IAT magmas (Beard 1986; Ishiwatari et al. 1990, 2003). For example, the clinopyroxene is more magnesian in an MORB series in comparison with an IAT series, at the same anorthite (An) content of the coexisting plagioclase (Ishiwatari et al. 2006). The clinopyroxene in basalt A has a lower Mg# than that from normal MORB, and clinopyroxene-plagioclase pairs of the samples have a close affinity to IAT (Fig. 10c). Therefore, the Ti, Cr, and Ca in clinopyroxene phenocrysts suggest "non-orogenic tholeiite" represented by MORB for basalt A, while on the other hand, the clinopyroxene Mg# vs. plagioclase An diagram give a clear indication that it is IAT rather than MORB. How can discrimination diagrams for whole-rock composition and clinopyroxene Mg# vs. plagioclase suggest that basalt A is volcanic arc tholeiitic basalt, whereas HFSE and REE show MORB-like nature in spidergram (Figs. 7a, 9, 10)? Lack of a negative Nb anomaly in the spidergram is also a significant characteristic of MORB-like rocks (Fig. 7a). Several authors reported "MORB-like tholeiitic fore-arc basalt (FAB)" from, for example, the Izu-Bonin-Mariana (IBM) arc, which closely resemble basalt A, in a number of features: high and uniform FeO*/MgO ratio (average 2.2); moderate TiO_2 (average 1.3 wt%); low LREE/HREE ratio (average 1.0); nearly identical HFSE and HREE concentrations to those of MORB; a flat chondrite-normalized REE pattern; and the absence of a negative Nb anomaly (e.g., Beccaluva et al. 2005; Dilek and Furnes 2003, 2014; Hickey-Vargas 1998; Ishizuka et al. 2009, 2011, 2014; Li et al. 2013; Reagan et al. 2010; Table 1; Fig. 7). It has been recognized that V

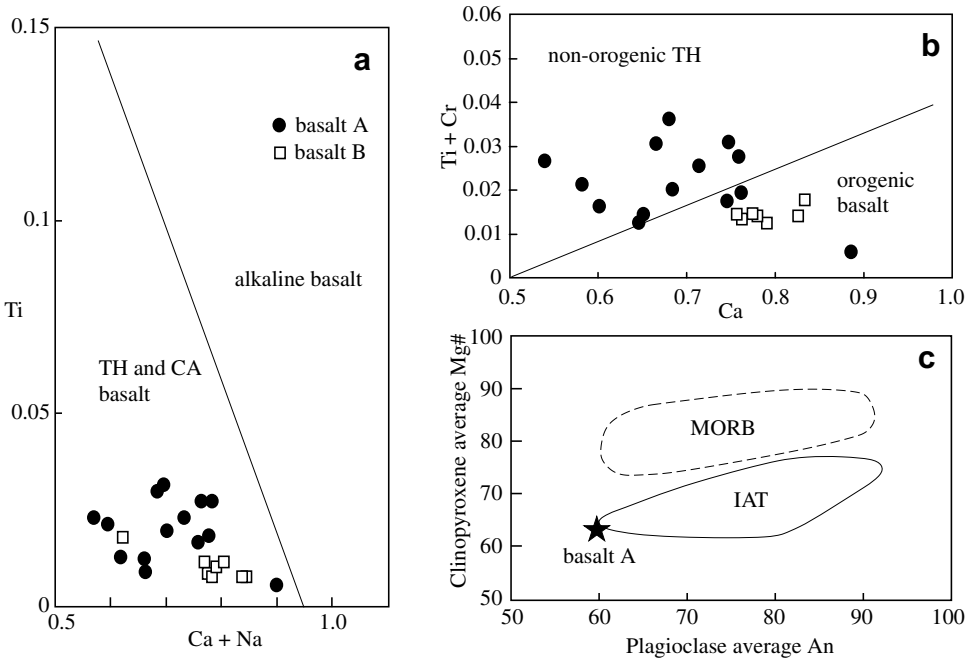

Fig. 10 Diagrams for clinopyroxene and plagioclase chemical compositions. **a, b** Diagrams for clinopyroxene phenocryst (Leterrier et al. 1982). The samples plotted in the field of "TH and CA basalt" are adaptive to the diagram (**b**). *TH* tholeiite, *CA* calc-alkaline. **c** Clinopyroxene Mg# (=100 Mg/(Fe + Mg)) and plagioclase An value (=100 Ca/(Na + Ca)) coexisting in the sample from basalt A. Nearly identical data were obtained from three samples of the basalt A from the pillow lava, and their average is shown here. Samples obviously have an affinity to the island arc tholeiite (IAT) rather than normal MORB. MORB and IAT fields are after Ishiwatari (1999) and Ishiwatari et al. (2006)

concentration and Ti/V ratio are significant factors to discriminate between FAB and typical IAT and MORB (e.g., Ishizuka et al. 2009; Reagan et al. 2010). FAB is known to have a comparatively high V concentration (generally more than 200 ppm) and to show a lower Ti/V ratio (commonly 10–20) than MORB (e.g., Ishizuka et al. 2009; Reagan et al. 2010). In addition, it generally shows a higher Ti/V ratio than IAT when V concentration is higher than ca. 350 ppm (e.g. Beccaluva et al. 2005; Ishizuka et al. 2011, 2014; Reagan et al. 2010; Fig. 11). In the present samples, a V concentration of 364–456 ppm and a Ti/V ratio of between 18 and 21 suggest an affinity to FAB but not to normal MORB or IAT (Fig. 11). When the basalt A samples are plotted on the V vs. Ti/1000 diagram (Fig. 11), they overlap with the field of FAB and back-arc basin basalt (BABB). However, most BABB has a Ti/V ratio of more than 20 (Shervais 1982), which suggests a higher probability of basalt A being FAB rather than BABB. In general, FAB has a lower LREE/HREE ratio in chondrite-normalized values than MORB or BABB from the Philippine Sea Basin (Hickey-Vargas 1998; Ishizuka et al. 2009, 2014), and it lacks a clear enrichment in LILE compared to REE and HFSE, implying it received little or no input from slab-derived material (Ishizuka et al. 2014). However, basalt A differs from this in showing a slightly higher LREE/HREE ratio than MORB, and in being enriched in LILE (e.g., Rb and Ba) compared with HFSE and REE (Table 1; Fig. 7a). LILE- and/or LREE-enriched FAB, such as those from the DSDP sites 458 and 459 and from the Albanide–Hellenide orogenic belt in the Balkans, is considered to have been formed as a result of the modification of the melt source by subduction-derived fluids (Beccaluva et al. 2005; Reagan et al. 2010) and the inference is that this may also be the case for basalt A.

Tectonic setting of basalt B

The HFSE vs. La/Yb diagrams suggest a high possibility of calc-alkaline basalt (CAB) for the samples (Nakamura et al. 2000; Fig. 8). Basalt B is plotted in the fields of the MORB or LPT or CAB in the Ti–Zr–Y diagram (Pearce and Cann 1973; Fig. 9c). In other words, this basalt is characteristic of MORB or arc basalt from magma of low-to-medium-potassium series. Discrimination diagrams using Ti, Zr, and Y tell us that basalt B is volcanic arc basalt (Pearce 1982, 1983; Fig. 9a, b). The trend in the spidergram, showing an enrichment in LILE compared with HFSE, supports the results of the Ti, Zr, and Y examination (Pearce 1983; Fig. 7a). A pronounced negative Nb and Ta anomaly in the spidergram also suggests volcanic arc basalt (Fig. 7a). The chondrite-normalized REE patterns with a gradual HREE depletion are similar to those of CAB (Nakamura et al. 2000 and references therein, Fig. 7b). The SiO_2 vs. FeO*/MgO (Miyashiro 1974) and MnO–TiO_2–P_2O_5 (Mullen 1983) diagrams indicate CAB for basalt B (Fig. 9d, e). This basalt is similar to calc-alkaline rocks, such as those of the Bonin Islands, in terms of its distinctive LILE-enrichment, Nb depletion, moderate V concentration, and low Ti/V ratio (Ishizuka et al. 2014; Shervais 1982; Figs. 7a, 11). The Ti vs. (Ca + Na) diagram for clinopyroxene phenocryst

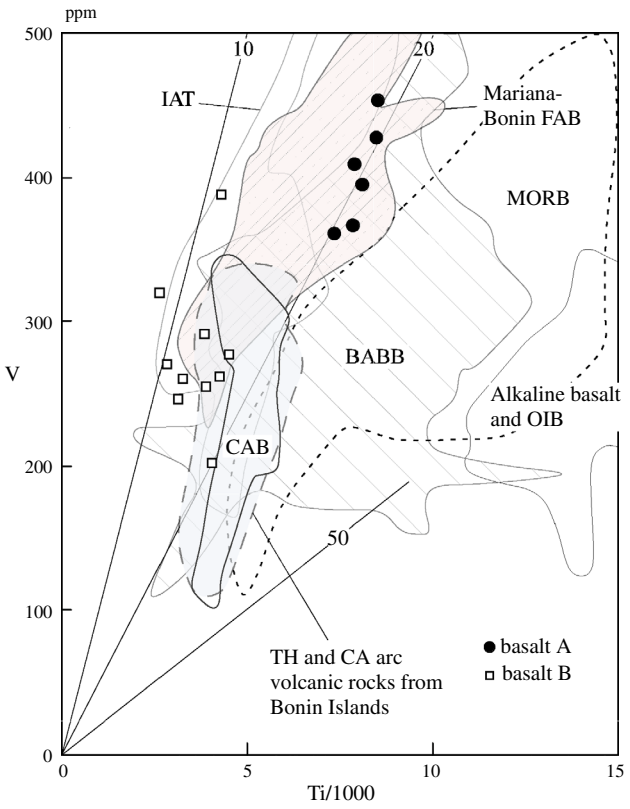

Fig. 11 V vs. Ti/1000 diagram (Shervais 1982). The IAT, CAB, BABB, MORB, Alkaline basalt, and OIB fields are after Shervais (1982), and others are after Ishizuka et al. (2014). The diagram suggests that the basalt A is fore-arc basalt (FAB) rather than normal MORB. Although the basalt A is plotted in the overlapped field of the FAB and back-arc basin basalt (BABB), the majority of the BABB (85% data within Shervais 1982) is more than 20 in Ti/V ratio; therefore, the basalt A is more probable to FAB than BABB. *IAT* typical island arc tholeiite, *OIB* oceanic island basalt, *CAB* calc-alkaline basalt, *TH* tholeiite, *CA* calc-alkaline

(Leterrier et al. 1982) clearly indicates that basalt B is non-alkaline. The (Ti+Cr) vs. Ca diagram (Leterrier et al. 1982) suggests "orogenic basalt", including island arc tholeiitic, calc-alkaline, and shoshonitic basalts (Fig. 10). Thus, it is probable that this basalt is CAB, as a result of an examination of both whole-rock and clinopyroxene chemistries. Most basalt B samples, 092014, 092709, Iw 6a, Iw 6b, 930706c, 072201, and 072204, resemble the high-Mg basalt of the Miocene Northeast Japan arc in their high MgO (average 8.5 wt%), high Cr (average 193 ppm), and low FeO*/MgO ratio (average 1.2) (Shuto et al. 1985, 2015; Takimoto and Shuto 1994; Table 1), and the latter two samples seem to be ankaramite in high CaO concentration. Sample 930706c is picritic with 11.6 wt% in MgO, 238 ppm in Cr, and 149 ppm in Ni. The conclusion is that the basalt B is of CAB, and some samples are probably high-Mg CAB.

Petrologic-tectonic variation of the Hitoegane succession

The chondrite-normalized REE patterns clearly demonstrate that basalt B has a much higher LREE/HREE ratio than basalt A and that basalt A has higher HREE concentrations than basalt B (Fig. 7b). These facts suggest that basalts A and B were formed by different magmatic processes. Both the spidergram and the discrimination diagrams seem to show that the FAB volcanism that gave rise to basalt A and the calc-alkaline volcanism resulting in basalt B took place in a volcanic arc. With this background, the environmental variation of the Hitoegane succession will now be discussed. In the Iwatsubodani Formation, pyroclastic rock that includes abundant clasts of basalt B with minor amounts of basalt A overlies pillow lava entirely composed of basalt (A) The chemical composition of basalt B, which forms the majority of the clasts in the pyroclastic rock, reflects the volcanism of the pyroclastic rock, and the composition of basalt A, which forms the pillow lava, indicates a slightly earlier volcanism than the volcanism of basalt (B). In other words, the early FAB volcanism that gave rise to basalt A was followed by the high-Mg calc-alkaline volcanism of basalt B.

The stratigraphic succession composed of FAB, boninite, and high-Mg andesite, and tholeiitic/calc-alkaline volcanic rocks in ascending order has been reported worldwide from supra-subduction zones (SSZ) (e.g., Beccaluva et al. 2005; Dilek and Furnes 2003; Ishizuka et al. 2014). The Iwatsubodani Formation with FAB and overlying high-Mg CAB is quite similar to this standard succession, although the boninite series is absent. It should be noted, however, that high-Mg andesite (58 wt% SiO_2, 0.90 wt% TiO_2, 5.5 wt% MgO and 1.3 FeO*/MgO ratio) and boninitic rock (53 wt% SiO_2, 0.49 wt% TiO_2, 8.5 wt% MgO and 1.1 FeO*/MgO ratio) were obtained from river boulders in the upper reaches of the Iwatsubodani Valley (Fig. 4; Tsukada, unpublished data). It follows that high-Mg andesite and boninite are likely to occur in the Iwatsubodani Formation, but this remains to be confirmed, because the geological relationship between the "High-Mg andesite and boninite" and this formation is still uncertain. Based on lithological, chronological, and geochemical examination, the model proposed is that FAB is erupted at the earliest stage of island arc formation (the initial stages of subduction) and that subsequently boninitic/tholeiitic/calc-alkaline arc volcanism occur at an SSZ (e.g., Dilek and Furnes 2014; Ishiwatari et al. 2006; Ishizuka et al. 2014; Li et al. 2013). If this model is applied to the Iwatsubodani Formation, the basalt A (FAB) probably represents the early Paleozoic subduction initiation volcanism and the overlying basalt B (high-Mg CAB) represents the subsequent arc volcanism at an SSZ.

The Iwatsubodani Formation is entirely composed of mafic volcanic rocks, but in contrast, the overlying Hitoegane Formation includes large amounts of felsic tuff and tuffaceous clastic rocks yielding *Periodon* conodonts, which is thought to suggest an open-ocean or continental slope environment (e.g., Armstrong et al. 2001; Dubinina and Ryazantsev 2008; Tsukada 1997; Tsukada and Koike 1996; Fig. 4). The lower part of the Hitoegane Formation intercalates mafic pyroclastic rock layers similar to those of the Iwatsubodani Formation (Tsukada 1997), and this suggests a conformable/unconformable relationship between the Iwatsubodani and Hitoegane Formations, as previously discussed. The zircon U-Pb age of ca. 472 Ma from the lowest horizon of the Hitoegane Formation suggests that the volcanic transition from mafic to felsic was likely to have occurred around the early or middle Ordovician (International Commission on Stratigraphy 2015; Nakama et al. 2010). The upper part of the Hitoegane Formation yields upper Silurian radiolarians (*Pseudospongoprunum tauversi and Futobari solidus–Zadrappolus tenuis* assemblages) and contemporaneous zircons of ca. 426 Ma (Manchuk et al. 2013b). The upper Silurian tuffaceous rocks of the Fukuji succession in the Fukuji area, 3 km west of the study area (Fig. 3), yields radiolarians of the *Futobari solidus–Zadrappolus tenuis* assemblage and contemporaneous zircons of ca. 421 Ma (Manchuk et al. 2013a). This lithological, paleontological, and chronological evidence strongly suggests that the upper Silurian tuffaceous rocks of the Fukuji succession are correlated with a part of the Hitoegane Formation (Manchuk et al. 2013b; Fig. 2).

Regional correlation of the Hitoegane succession

The previous section proposed that the Hitoegane succession, composed mainly of mafic volcanic rock (Iwatsubodani Formation) and clastic and felsic tuffaceous rocks (Hitoegane Formation), was formed at an early Paleozoic volcanic arc at an SSZ. Here, the regional correlation of the Hitoegane succession will be examined with a key word, i.e., an early Paleozoic volcanic arc at an SSZ.

The lower Paleozoic Oeyama ophiolite that structurally overlies the rocks of the Renge metamorphic rocks and Akiyoshi, Maizuru, and Mino–Tamba belts is sporadically exposed in the Sangun–Renge belt, Chugoku Mountains, west of Hida Gaien belt, southwest Japan (Fig. 1). The Oeyama ophiolite is composed mainly of residual peridotite with podiform chromite deposits and minor gabbroic rocks, while mafic volcanic rocks are not yet found (e.g., Ishiwatari and Tsujimori 2003). Amphibolite and jadeitite occur as blocks or dykes in places (e.g., Ehiro et al. 2016; Kurokawa 1985; Nishimura and Shibata 1989; Tsujimori and Liou 2004). The chemical composition of spinel in peridotite and chromite suggests back-arc basin or primitive oceanic arc origin for this ophiolite (e.g., Arai and Yurimoto 1995; Ishiwatari 1989; Tsujimori and Itaya 1999). Ehiro et al. (2016) proposed that this ophiolite had acted as a fore-arc mantle wedge and as a basement for lower Paleozoic fore-arc basin formations. Jadeitite within the ophiolite showing high-pressure and low-temperature metamorphism probably suggests a fore-arc mantle wedge at an SSZ (Ehiro et al. 2016; Stern et al. 2013; Harlow et al. 2015). In either scenario, it is now accepted that the Oeyama ophiolite is of volcanic arc origin at an SSZ. Gabbroic intrusive rock in the ophiolite gives Sm–Nd isochron ages of ca. 560 Ma (Hayasaka et al. 1995), and jadeitite yields hydrothermal zircon U–Pb ages ranging from ca. 520 to 450 Ma (Ehiro et al. 2016; Tsujimori et al. 2005; Kunugiza and Goto 2010). In addition, peridotite and amphibolite/metagabbro block in the peridotite give hornblende K–Ar ages of ca. 464–444 Ma, and ca. 443–403 Ma, respectively (Nishimura and Shibata 1989; Tsujimori 1999; Tsujimori et al. 2000; Tsujimori and Ishiwatari 2002). Ishiwatari and Tsujimori (2003) regarded this ophiolite as Cambro–Ordovician. In summary, the Oeyama ophiolite, located between the Hida and Mino–Tamba belts, is considered to have been formed at a volcanic arc at an SSZ in the early Paleozoic, as is the case with the Iwatsubodani Formation of the Hida Gaien belt. Sugamori and Ishiwatari (2015) proposed a model in which the Permian marginal sea (called the Maizuru Ocean) was formed as a result of back-arc-spreading which split the older arc crust that constituted the "proto-Oeyama ophiolite." Further they speculated that the Oeyama ophiolite and the back-arc spreading-related Permian ophiolite (the present Yakuno ophiolite in the Maizuru belt, e.g., Ichiyama and Ishiwatari 2004), are the "fossilized remains" of the Paleozoic arc–marginal sea system which had existed for 300 million years. This Paleozoic arc–marginal sea system might have been generated by the subduction of an oceanic plate which was initiated in the early Paleozoic as evidenced by the basaltic rocks reported here.

The lithostratigraphic similarity between the Hitoegane succession and the Hayachine–Miyamori ophiolite and covering formations (called the H-M succession, here) of the South Kitakami belt, northeast Japan, has been pointed out (e.g., Ehiro et al. 2016; Tazawa 1993; Tsukada and Koike 1997; Fig. 1). The Hayachine–Miyamori ophiolite is composed mainly of peridotite, pyroxenite, hornblendite, gabbro, and mafic volcanic rocks (e.g., Ehiro et al. 2016; Ozawa et al. 2015). The Hayachine–Miyamori ophiolite has a common petrologic feature, namely, the presence of hornblende as a major constituent mineral in both mafic and ultramafic rocks, which suggests a hydrous condition for the ophiolite formation (Ozawa 1984, 1988). At one time, this was inferred to have been formed in a rift zone (e.g., Osawa 1983), however, it was pointed out that the geochemical and petrological features suggest an arc environment rather than

MORB equivalents (e.g., Mori et al. 1992; Ozawa 1984). Ozawa et al. (2015) proposed that the Hayachine–Miyamori ophiolite is divided into the back-arc "Hayachine complex" and the fore-arc "Miyamori complex." Ozawa et al. (2015) considered that the aluminous spinel ultramafic suite (ASUS) in the Hayachine complex underwent melting in the back-arc region and that the ASUS and chromite-bearing ultramafic suite of the Miyamori complex underwent melting closer to the fore-arc region. In the opinion of Ozawa et al. (2015), however, these complexes are not two separate ophiolites that are genetically unrelated to each other, but rather that they share the same arc–back-arc system in an SSZ. Such a back-arc origin for the Hayachine complex is consistent with the conclusions of Ehiro and Kanisawa (1999) and Uchino and Kawamura (2016). Shibata and Ozawa (1992) reported a 510 ± 70 Ma Sm–Nd whole-rock isochron age for the Miyamori complex, and Yoshikawa and Ozawa (2007) presented a clinopyroxene Sm–Nd model age of 499 ± 65 Ma. Yoshikawa et al. (2012) obtained a clinopyroxene Sm–Nd isochron of 490 ± 60 Ma from the Hayachine and Miyamori complexes, and Ozawa et al. (1988) and Shibata and Ozawa (1992) estimated, based on hornblende K–Ar method, the cooling age of this ophiolite as 400–500 Ma. Zircon LA-ICP-MS U–Pb ages of 466 ± 6 Ma and 457 ± 10 Ma were obtained from the trondhjemite and the felsic tuff of the Hayachine complex (Shimojo et al. 2010). Taking all these together, the ages by hornblende K–Ar, hornblende Sm–Nd, clinopyroxene Sm–Nd, and Zircon U–Pb methods, therefore, give a concentration at 400–500 Ma (Ozawa et al. 2015). It has generally been considered that the Ordovician to Silurian clastic rocks and felsic tuffaceous rocks (Yakushigawa Formation) conformably cover the Hayachine complex (e.g., Ehiro et al. 2016). However, Shimojo et al. (2010) proposed an unconformable relationship between the Hayachine complex and the Yakushigawa Formation on the grounds that detrital zircons of ca. 425 Ma are contained in the lower part of this formation. Upper rocks (the Odagoe Formation and its equivalent) of the Yakushigawa Formation yield Silurian coral, trilobites, and brachiopods (e.g., Ehiro et al. 1986, 2016; Okami et al. 1986). Ozawa et al. (2015) concluded that the Hayachine–Miyamori ophiolite was formed at an Ordovician SSZ arc–back-arc system and that subsequently Ordovician (?)–Silurian felsic volcanism occurred at this area as evidenced by the Yakushigawa and Odagoe Formations.

The Hayachine–Miyamori ophiolite was formed at early Paleozoic volcanic arc at an SSZ as was the case for the Iwatsubodani Formation, as mentioned above. In addition, it has been pointed out that there is a strong stratigraphic similarity between the H-M succession and the Hitoegane succession: the Hayachine–Miyamori ophiolite is overlain by the Ordovician (?) or Silurian clastic and felsic tuffaceous rocks, and similarly, the Hitoegane succession is composed of basalt (Iwatsubodani Formation) and the overlying Ordovician–Silurian clastic and felsic tuffaceous rocks (Hitoegane Formation) (e.g., Tazawa 1993; Tsukada and Koike 1997).

Accordingly, the H-M succession and the Hitoegane succession are quite likely correlated in the similarity of their ages (Early Paleozoic), their tectonic settings (arc volcanism at SSZ), and their environmental variations (mafic volcanism and following felsic volcanism). Okawa et al. (2013) reported Precambrian detrital zircons from the Yakushigawa Formation and its equivalent, and assumed that these formations were formed near a continental magmatic arc having Precambrian basement rocks, at around northern East Gondwana.

A similarity between the Oeyama ophiolite, the Hayachine–Miyamori ophiolite, and the Sergeevka ophiolite (Promorye, Far East Russia) has been recognized in many aspects (e.g., Ishiwatari and Tsujimori 2003; Fig. 1). The Sergeevka ophiolite structurally overlies the younger blueschist-facies metamorphic rocks (Shaiginskiy blueschist) and Jurassic–Cretaceous accretionry complexes (Samarka terrane). The Shaiginskiy blueschist and Samarka terrane correspond to the Renge metamorphic rocks and the Mino–Tamba belt of Southwest Japan, respectively, and the Sergeevka and Oeyama ophiolites share the same structural position in that they both overlie the blueschist-facies metamorphic rocks and Mesozoic accretionry complexes (e.g., Ishiwatari and Tsujimori 2003; Kojima 1989; Kojima et al. 2000). The Sergeevka ophiolite is composed mainly of gneissose hornblende metagabbro and gives a zircon U-Pb age of 528–493 Ma (Khanchuk et al. 1996). Mishkin et al. (1970) reported muscovite with a K-Ar age of 529 Ma and hornblende K–Ar age of 622 Ma, whereas Ishiwatari and Tsujimori (2003) presented hornblende K–Ar ages of 470–430 Ma. The conclusion is that the Segeevka, Oeyama, and Hayachine–Miyamori ophiolites are correlated with each other in that they have a similar structural position, lithology, and age (Ishiwatari and Tsujimori 2003).

As has been mentioned, the Iwatsubodani Formation of the Hida Gaien belt and the Oeyama ophiolite is probably comparable to each other. Thus, if the Oeyama ophiolite is a relative of the Sergeevka ophiolite, the Iwatsubodani Formation also might be the equivalent of the Sergeevka body. Besides, the Hitoegane succession corresponds to the H-M succession in environmental variation: early Paleozoic SSZ mafic arc volcanism followed by felsic volcanism. Consequently, the evidence points to the fact that the Hitoegane succession of the Hida Gaien belt, the Oeyama ophiolite, the H-M succession, and the Sergeevka ophiolite probably shared an oceanic arc system at an SSZ near a continental margin in the early Paleozoic.

Acknowledgements We would like to express our thanks to the late Emeritus Prof. E. Horikoshi and to Emeritus Prof. O. Ujike of the University of Toyama for their critical advice. We would also like to thank Prof. S. Otoh of the University of Toyama and Prof. M. Adachi, Prof. M. Takeuchi, and Prof. H. Yoshida at Nagoya University for helpful discussion. We appreciate critical review comments from Dr. A. Ishiwatari of the Nuclear Regulation Authority of Japan and an anonymous reviewer, which greatly improved an earlier draft of this manuscript. Special thanks go to Mr. S. Yogo, Ms. M. Nozaki, Dr. Y. Asahara, Dr. H. Hasegawa, and Dr. K. Naemura at Nagoya University for their technical support. We are grateful to Dr. Giles Clarke for his helpful criticism of the manuscript.

References

Adachi S (1985) Smaller foraminifers of the Ichinotani Formation (Carboniferous—Permian), Hida Massif, Central Japan. Sci rep Inst Geosci, University of Tsukuba B 6:59–139

Anders E, Grevesse N (1989) Abundances of the elements: meteoritic and solar. Geochim Cosmochim Acta 53:197–214

Arai S, Yurimoto H (1995) Possible sub-arc origin of podiform chromitites. Isl Arc 4:104–111

Armstrong HA, Floyd JD, Barron HF (2001) Conodont biostratigraphy of the Crawford Group, Southern Uplands. British Geol Surv Res Rep, RR/01/05

Beard JB (1986) Characteristic mineralogy of arcrelated cumulate gabbros: Implications for the tectonic setting of gabbroic plutons and for andesite genesis. Geology 14:848–851

Beccaluva L, Coltorti M, Saccani E, Siena F (2005) Magma generation and crustal accretion as evidenced by supra-Magma generation and crustal accretion as evidenced by supra-suprasubduction ophiolites of the Albanide–Hellenide Subpelagonian zone. Isl Arc 14:551–563

Charvet J (2012) Late Paleozoic–Mesozoic tectonic evolution of SW Japan: a review—reappraisal of the accretionary orogeny and revalidation of the collision model. J Asian Earth Sci 72:75–87

Dilek Y, Furnes H (2003) Arc trench rollback and forearc accretion: 2. A model template for ophiolites in Albania, Cyprus, and Oman. In: Dilek Y, Robinson P (eds) Ophiolites in Earth History. Geol Soc London Sp Pub 218:43–68

Dilek Y, Furnes H (2014) Ophiolites and their origins. Elements 10:93–100

Dubinina SV, Ryazantsev AV (2008) Conodont stratigraphy and correlation of the Ordovician volcanogenic and volcanogenic sedimentary sequences in the South Urals. Rus J of Earth Sci 10:1–31

Ehiro M, Kanisawa S (1999) Origin and evolution of the South Kitakami Microcontinent during the Early–Middle Palaeozoic. In: Metcalfe I (ed) Gondwana dispersion and Asian accretion: IGCP 321 final results volume. A. A. Balkema, Rotterdam, pp 283–295

Ehiro M, Tazawa J, Oishi M, Okami K (1986) Discovery of *Trimerella* (Silurian Brachiopoda) from the Odagoe Formation, south of Mt. Hayachine in the Kitakami Massif, Northeast Japan and its significance. J Geol Soc Jap 92:753–756

Ehiro M, Tsujimori T, Tsukada K, Nuramkhaan M (2016) Basement rocks and associated cover. In: Moreno T, Wallis S, Kojima S, Gibbons W (eds) The geology of Japan. Geol Soc, London. pp 25–60

Faure M, Charvet J (1987) Late Permian/early Triassic orogeny in Japan: piling up of nappes, transverse linearion and continental subduction of the Honshu block. Earth Planet Sci Lett 84:295–308

Faure M, Caridroit M, Charvet J (1986) The Late Jurassic oblique collisional orogen of SW Japan: new structural data and synthesis. Tectonics 5:1089–1114

Gill JB (1981) Orogenic andesites and plate tectonics. Springer, p 390

Harlow GE, Tsujimori T, Sorensen SS (2015) Jadeitites and plate tectonics. Ann Rev Earth Planet Sci 43:105–138

Hayasaka Y, Sugimoto T, Kano T (1995) Ophiolitic complex and metamorphic rocks in the Niimi-Katsuyama area, Okayama Prefecture. Excursion Guide 102th Ann Meet Geol Soc Jap, pp 71–87

Hickey-Vargas R (1998) Origin of the Indian Ocean-type isotopic signature in basalts from Philippine Sea plate spreading centers: an assessment of local versus large-scale processes. J Geophys Res: Solid Earth 103:20963–20979

Horikoshi E, Tazawa J, Naito N, Kaneda J (1987) Permian brachiopods from Moribu, north of Takayama City, Hida Mountains, central Japan. J Geol Soc Jap 93:141–143

Ichiyama Y, Ishiwatari A (2004) Petrochemical evidence for off-ridge magmatism in a back-arc setting from the Yakuno ophiolite, Japan. Isl Arc 13:157–177

Igo H (1956) On the Carboniferous and Permian of the Fukuji district, Hida Massif, with special reference to the fusulinid zones of the Ichinotani Group. J Geol Soc Jap 62:217–240

Igo H (1960) First discovery of non-marine sediments in the Japanese Carboniferous. Proc Jap Acad 36:498–502

Igo H (1990) Paleozoic strata in the Hida "Gaien" Belt. In: Ichikawa K, Hara I, Hada S, Yao A (eds) Pre-Cretaceous Terranes of Japan, IGCP Project No 224: Pre-Jurassic Evolution of Eastern Asia, Osaka, pp 41–48

Igo H, Adachi S (1981) Foraminiferal biostratigraphy of the Ichinotani Formation (Carboniferous–Permian), Hida Massif, Central Japan Part 1—Some foraminiferas from the upper part of the Lower Member of the Ichinotani Formation. Sci rep Inst Geosci Univ Tsukuba. 2:101–118

International Commission on Stratigraphy (2015) International Chronostratigraphic Chart, v2015/01. International Union of Geological Sciences, Beijing

Ishiwatari A (1989) Ophiolites of Japan. J Geogr (Chigaku Zasshi) 98:290–303

Ishiwatari A (1999) Fragment of Paleozoic oceanic island arc crust in the Inner Zone of southwestern Japan: The Kamigori metagabbro body, Hyogo Prefecture. Mem Geol Soc Jap 52:273–285

Ishiwatari A, Tsujimori T (2003) Paleozoic ophiolites and blueschists in Japan and Russian Primorye in the tectonic framework of East Asia: a synthesis. Isl Arc 12:190–206

Ishiwatari A, Ikeda Y, Koide Y, (1990) Yakuno ophiolite, Japan: Fragments of Permian island arc and marginal basin crust with a hot spot. In: Malpas J, Moores E, Panayiotou A, Xenophontos C (eds) Ophiolites: Oceanic Crustal Analogues, Proceedings of the Troodos 1987 Symposium, Geological Survey Department, Nicosia, Cyprus, pp 497–506

Ishiwatari A, Sokolov SD, Vysotskiy SV (2003) Petrological diversity and origin of ophiolites in Japan and Far East Russia with emphasis on depleted harzburgite. In: Dilek Y, Robinson PT (eds) Ophiolites in Earth History, Geol Soc London Sp Pub, vol 218, pp 597–618

Ishiwatari A, Yanagida Y, Li Y-B, Ishii T, Haraguchi S, Koizumi K, Ichiyama Y, Umaka M (2006) Dredge petrology of the boninite- and adakite-bearing Hahajima Seamount of the Ogasawara (Bonin) forearc: an ophiolite or a serpentinite seamount? Isl Arc 15:102–118

Ishizuka O, Yuasa M, Taylor RN, Sakamoto I (2009) Two contrasting magmatic types coexist after the cessation of back-arc spreading. Chem geol 266:274–296

Ishizuka O, Tani K, Reagan KM, Kanayama K, Umino S, Harigane Y, Sakamoto I, Miyajima Y, Yuasa M, Dunkley JD (2011) The

timescales of subduction initiation and subsequent evolution of an oceanic island arc. Earth and Planet Sci Lett 306:229–240
Ishizuka O, Tani K, Reagan KM (2014) Izu–Bonin–Mariana Forearc Crust as a modern ophiolite Analogue. Elements 10:115–120.
Isozaki Y, Maruyama S, Fukuoka F (1990) Accreted oceanic materials in Japan. Tectonophys 181:179–205
Kamei T (1952) The stratigraphy of the Fukuji district, southern part of Hida Mountainland (Study on Paleozoic rocks of Hida 1). J Fac Liberal Arts Shinshu Univ 2:43–74
Kato M (1959) Some Carboniferous rugose corals from Ichinotani Formation, Japan. J Fac Sci Hokkaido Univ 10:263–287
Khanchuk AI, Ratkin VV, Ryazansteva MD, Golozubob VV, Gonokhova NG (1996) Geology and mineral deposits of Primorskiy Krai, Dalnauka, Vladivostok
Kojima S (1989) Mesozoic terrane accretion in northeast China, Sikhote-Alin and Japan regions. Palaeogeogr Palaeoclim Palaeont 69:213–232
Kojima S, Kemkin IV, Kametaka M, Ando A (2000) A correlation of accretionary complexes of Southern Sikhote-Alin of Russia and the Inner zone of Southwest Japan. Geosci J 4:175–185
Kunugiza K, Goto A (2010) Juvenile Japan: hydrothermal activity of the Hida-Gaien belt indicating initiation of subduction of proto-pacific plate in c. 520 Ma. J Geogr (Chigaku Zasshi) 119:279–293
Kurihara T (2007) Uppermost Silurian to Lower Devonian radiolarians from the Hitoegane area of the Hida-gaien terrane, central Japan. Micropaleont 53:221–237
Kurokawa K (1985) Petrology of the Oeyama ophiolitic complex in the Inner Zone of Southwest Japan. Sci Rep Niigata Univ (Ser E) 6:37–113
Leterrier J, Maury CR, Thonon P, Girard D, Marchal M (1982) Clinopyroxene composition as a method of identification of the magmatic affinities of paleo-volcanic series. Earth Planet Sci Lett 59:139–154
Li Y-B, Kimura J-I, Machida S, Ishii T, Ishiwatari A, Maruyama S, Qiu H-N, Ishikawa T, Kato Y, Haraguchi S, Takahata N, Hirahara Y, Miyazaki T Beccaluva (2013) High-Mg adakite and low-Ca boninite from a Bonin fore-arc seamount: implications for the reaction between slab melts and depleted mantle. J Petrol 54:1149–1175
Manchuk N, Horie K, Tsukada K (2013a) SHRIMP U-Pb age of the radiolarian-bearing Yoshiki Formation in Japan. Bul Geosci (Czechoslovakia) 88:223–240
Manchuk N, Kurihara T, Tsukada K, Kochi Y, Obara H, Fujimoto T, Orihashi Y, Yamamoto K (2013b) U-Pb zircon age from the radiolarian-bearing Hitoegane Formation in the Hida Gaien Belt, Japan. Isl Arc 22:494–507
Mishkin MA, Lelikov EP, Ovcharek EC (1970) New evidence of metamorphic rocks on the Japan Sea coast of southern Primorye. Dokl Akad Nauk 190:1426–1429
Miyashiro A (1974) Volcanic rock series in island arcs and active continental margins. Am J Sci 274:324–355
Miyashiro A, Kushiro I (1975) Petrology, vol 2. Kyoritsu shuppan, Tokyo
Mori K, Okami K, Ehiro M (1992) Paleozoic and Mesozoic sequences in the Kitakami Mountains (29th IGC Field Trip A05). In: Adachi M, Suzuki K (eds) 29th IGC field trip guide book 1 Paleozoic and Mesozoic terranes: basement of Japanese Islands Arcs. Nagoya University, Nagoya, pp 81–114
Mullen ED (1983) $MnO/TiO_2/P_2O^5$: a minor element discriminant for basaltic rocks of oceanic environments and its implications for petrogenesis. Earth Planet Sci Lett 62:53–62
Nakama T, Hirata T, Otho S, Maruyama S (2010) The oldest sedimentary age 472 Ma (Latest Early Ordovician) from Japan: U-Pb zircon age from the Hitoegane Formation in the Hida Marginal Belt. J Geogr (Chigaku Zasshi) 119:270–278
Nakamura K, Fujinaga K, Kato Y (2000) Rear earth element geochemistry of in-situ basalts from the Upper Cretaceous Shimanto Belt and its implication for their origin. Jpn Mag Min Petrol Sci 29:175–190
Niikawa I (1980) Geology and biostratigraphy of the Fukuji district, Gifu Prefecture, Central Japan. J Geol Soc Jap 86:25–36
Nishimura Y, Shibata K (1989) Modes of occurrence and K–Ar ages of metagabbroic rocks in the 'Sangun metamorphic belt', Southwest Japan. Mem Geol Soc Jap 33:343–357
Niwa M, Hottta K, Tsukada K (2004) Fusulinoideans from the Moribu Formation in the Hida-gaien Tectonic Zone, Nyukawa Village, Gifu Prefecture, central Japan. J Geol Soc Jap 110:384–387
Okami K, Ehiro M, Oishi M (1986) Geology of the Lower-Middle Palaeozoic around the northern marginal part of the Southern Kitakami Massif with reference to the geologic development of the 'Hayachine Tectonic Belt'. Essays in Geology., Professor Nobu Kitamura CommemorativeVolume, pp 313–330
Okawa H, Shimojo M, Orihashi Y, Yamamoto K, Hirata T, Sano S, Ishizaki Y, Kouchi Y, Yanai S, Otoh S (2013) Detrital zircon geochronology of the Silurian–Lower Cretaceous continuous succession of the South Kitakami belt, northeast Japan. Mem Fukui Pref Dinosaur Mus 12:35–78
Okazaki Y (1974) Devonian trilobites from the Fukuji Formation in the Hida Massif, central Japan. Mem Fac Sci Kyoto Univ (Geol and Min) 40:84–94
Osawa M (1983) Geological studies on the 'Hatachine Tectonic Belt'. Cont Inst Geol Paleont Tohoku Univ 85:1–30
Otoh S, Tsukada K, Kasahara K, Hotta K, Sasaki M (2003) Outline of the shear zones in the Hida Marginal Belt. Mem Fukui Pref Dinosaur Mus No 2:63–73
Ozawa K (1984) Geology of the Miyamori ultramafic complex in the Kitakami Mountains, northeast Japan. J Geol Soc Jap 90:697–716
Ozawa K (1988) Ultramafic tectonite of the Miyamori ophiolitic complex in the Kitakami Mountains, Northeast Japan: Hydrous upper mantle in an island arc. Cont Min Petrol 99:159–175
Ozawa K, Shibata K, Uchiumi S (1988) K–Ar ages of hornblende in gabbroic rocks from the Miyamori ultramafic complex of the Kitakami Mountains. J Jap Min Petrol Econ Geol 83:150–159
Ozawa K, Maekawa H, Shibata K, Asahara Y, Yoshikawa M (2015) Evolution processes of Ordovician–Devonian arc system in the South-Kitakami Massif and its relevance to the Ordovician ophiolite pulse. Isl Arc 24:73–118
Pearce JA (1982) Trace element characteristics of lavas from destructive plate boundaries. In: Thorpe R (ed) Andesites. John Wiley and Sons, Chichester, p 525
Pearce JA (1983) Role of the sub-continental lithosphere in magma genesis at active continental margins. In: Hawkesworth CJ, Norry MJ (eds) Continental basalts and mantle Xenoliths. Shiva, Nantwich, Cheshire, pp 230–250
Pearce JA, Cann JR (1973) Tectonic setting of basic volcanic rocks determined using trace element analysis. Earth Planet Sci Lett 19:290–300
Pearce JA, Stern RJ (2006) Origin of Back-Arc Basin Magmas: Trace Element and Isotope Perspectives. In: Christie DM, Fisher CR, Lee S–M, Givens S (eds) Back-Arc Spreading Systems: Geological, Biological, Chemical, and Physical Interactions, Geophysical Monograph Series 166, The American Geophysical Union. pp 63–86
Pearce JA, Stern RJ, Bloomer SH, Fryer P (2005) Geochemical mapping of the Mariana arc–basin system: Implications for the nature and distribution of subduction components. Geochem Geophys Geosystem 6:Q07006. doi:10.1029/2004GC000895
Reagan KM, Ishizuka O, Stern JR, Kelley AK, Ohara Y, Blichert-Toft J, Bloomer HS, Cash J, Fryer P, Hanan BB, Hickey-Vargas R, Ishii T, Kimura J, Peate WD, Rowe CM, Woods M (2010)

Fore-arc basalts and subduction initiation in the Izu-Bonin-Mariana system. Geochem Geophys Geosystem 11:Q03 × 12, doi:10.1029/2009GC002871

Shervais WJ (1982) Ti-V plots and the petrogenesis of modern and ophiolitic lavas. Earth Planet Sci Lett 59:101–118

Shibata K, Ozawa K (1992) Ordovician arc ophiolite, the Hayachine and Miyamori ultramafic complexes, Kitakami Mountains, Northeast Japan: isotopic ages and geochemistry. Geochem J 26:85–97

Shimojo M, Otoh S, Yanai S, Hirata T, Maruyama S (2010) LA-ICP-MS U-Pb age of some older rocks of the South Kitakami Belt, Northeast Japan. J Geogr (Chigaku Zasshi) 119:257–269

Shuto K, Yashima R, Takimoto T (1985) Primitive olivine tholeiite from the Ryozen district, northeastern part of Fukushima Prefecture, Northeast Japan. J Jap Min Petr Econ Geol 80:55–72

Shuto K, Nohara-Imanaka R, Sato M, Takahashi T, Takazawa E, Kawabata H, Takanashi K, Ban M, Watanabe N, Fujibayashi N (2015) Across-arc variations in geochemistry of Oligocene to quaternary basalts from the NE Japan arc: constraints on source composition, mantle melting and slab input composition. J Petrol 56:2257–2294

Stern RJ, Tsujimori T, Harlow GE, Groat LA (2013) Plate tectonic gemstones. Geology 41:723–726

Sugamori Y, Ishiwatari A (2015) Discovery of serpentine gravel from the Ultra-Tamba Terrane in the Kawanishi City, Hyogo Prefecture, southwest Japan: relationship between the Oeyama ophiolite and "Maizuru arc". J Geol Soc Jap 121:391–401

Sun S-S, Mcdonough EF (1989) Chemical and isotopic systematical of oceanic basalts: implications for mantle composition and process. Geol Soc London Spec Pub 42:313–345.

Takebe M, Yamamoto K (2003) Geochemical fractionation between porcellanite and host sediment. J Geol 111:301–312

Takimoto T, Shuto K (1994) Petrology of Middle Miocene volcanic rocks from the Tomari area in the Shimokita Peninsula, Northeast Japan arc. Sci Rep Niigata Univ Ser E 9:25–88

Tashiro M, (1994) Cretaceous tectonic evolution of southwest Japan from the bivalve faunal view-points. Res Rep Kochi Univ Nat Sci 43:43–54

Tazawa J (1991) Middle Permian brachiopod biogeography of Japan and adjacent regions in East Asia. In: Ishii K, Liu X, Ichikawa K, Huang B (eds), Pre-Jurassic geology of Inner Mongolia, China, Report of China-Japan Cooperative Research Group 1987–1989, Matsuya Insatsu, Osaka, pp 213–230

Tazawa J (1993) Pre-Neogene tectonics of the Japanese Islands from the viewpoint of palaeobiogeography. J Geol Soc Jap 99:525–543

Tazawa J (2004) The strike-slip model; A synthesis on the origin and tectonic evolution of the Japanese Islands. J Geol Soc Jap 110:503–517

Tazawa J, Tsushima K, Hasegawa Y (1993) Discovery of Monodiexodina from the Permian Moribu Formation in the Hida Gaien Belt, Central Japan. Earth Sci (Chikyu-Kagaku) 47:345–348

Tazawa J, Niikawa I, Furuichi K, Miyake Y, Ohkura M, Furutani H, Kaneko N (1997) Discovery of Devonian tabulate corals and crinoids from the Moribu district, Hida Gaien Belt, central Japan. J Geol Soc Jap 103:399–401

Tazawa J, Hasegawa Y, Yoshida K (2000a) Schwagerina (Fusulinacean) and Choristites (Brachiopoda) from the Carboniferous Arakigawa Formation in the Hidagaien Belt, central Japan. Earth Sci (Chikyu-Kagaku) 54:196–199

Tazawa J, Yang W, Miyake Y (2000b) *Cyrtospirifer* and *Leptophloeum* from the Devonian Rosse Formation, Hida Gaien Belt, central Japan. J Geol Soc Jap 106:727–735

Tsujimori T (1999) Petrogenesis of the Fuko Pass high-pressure metacumulate from the Oeyama peridotite body, southwestern Japan: evidence for Early Paleozoic subduction metamorphism. Mem Geol Soc Jap 52:287–302

Tsujimori T, Ishiwatari A (2002) Granulite facies relics in the early Paleozoic kyanite-bearing ultrabasic metacumulate in the Oeyama belt, the Inner Zone of southwestern Japan. Gondwana Res 5:823–835

Tsujimori T, Itaya T (1999) Blueschist-facies metamorphism during Paleozoic orogeny in southwestern Japan: Phengite K–Ar ages of blueschist-facies tectonic blocks in a serpentinite mélange beneath early Paleozoic Oeyama ophiolite. Isl Arc 8:190–205

Tsujimori T, Nishina K, Ishiwatari A, Itaya T (2000) 403–443 Ma kyanite-bearing epidote amphibolite from the Fuko Pass metacumulate in Oeyama, the Inner Zone of southwestern Japan. J Geol Soc Jap 106:646–649

Tsujimori T, Liou JG, Wooden J, Miyamoto T (2005) U–Pb dating of large zircons in low-temperature jadeitite from the Osayama serpentinite melange, Southwest Japan: insights into the timing of serpentinization. Int Geol Rev 47:1048–1057

Tsukada K (1997) Stratigraphy and structure of Paleozoic rocks in the Hitoegane area, Kamitakara Village, Gifu Prefecture. J Geol Soc Jap 103:658–668

Tsukada K (2003) Jurassic dextral and Cretaceous sinistral movements along the Hida marginal belt. Gondwana Res 6:687–698

Tsukada K (2005) Tabulata corals from the Devonian Fukuji Formation, Hida gaien belt, central Japan—Part 1. Bul Nagoya Univ Mus No 21:57–125

Tsukada K, Koike T (1997) Ordovician conodonts from the Hitoegane area, Kamitakara village, Gifu prefecture. J Geol Soc Jap 103:171–174

Tsukada K, Takahashi Y (2000) Redefinition of the Permian strata in the Hida-gaien Tectonic Zone, Fukuji area, Gifu Prefecture, Central Japan. J Earth Planet Sci Nagoya Univ 31:1–35

Tsukada K, Takahashi Y, Ozawa T (1999) Stratigraphic relationship between the Mizuyagadani and Sorayama Formations, and age of the Sorayama Formation, in the Hida-gaien Tectonic Zone, Kamitakara Village, Gifu Prefecture, central Japan. J Geol Soc Jap 105:496–507

Tsukada K, Takeuchi M, Kojima S (2004) Redefinition of the Hida Gaien belt. J Geol Soc Jap 110:640–658

Uchino T, Kawamura M (2016) Ordovician backarc-basin metadolerite and metabasalt of the South Kitakami Terrane, Northeast Japan. Isl Arc 25:274–286

Ujike O (1989) Geochemical magma-type discrimination diagrams: a case study on Miocene basaltic rocks from northeastern Japan. Bull Volcanol Soc Jap II 34:157–168

Wakita K (1989) Accretionary tectonics in Japan. Bull Geol Surv Jap 40:251–253

Wakita K, Okamura Y, Awata Y (1992) Tectonic Map of Japan. In Geological Survey of Japan (ed) Geological Atlas of Japan, 2nd edn. Asakura Publishing, Tokyo

Watanabe K (1991) Fusuline biostratigraphy of the Upper Carboniferous and Lower Permian of Japan, with special reference to the Carboniferous-Permian boundary. Paleont Soc Jap SP 32:1–150

Yamakita S, Otoh S (2000) Cretaceous rearrangement processes of pre-Cretaceous geologic units of the Japanese Islands by MTL-Kurosegawa left-lateral strike-slip fault system. Mem Geol Soc Jap No 56:23–38

Yamamoto K, Morishita T (1997) Preparation of standard composites for the trace element analysis by X-ray fluorescence. J Geol Soc Jap 103:37–45

Yamamoto K, Yamashita F, Adachi M (2005) Precise determination of REE for sedimentary reference rocks issued by the Geological Survey of Japan. Geochem J 39:289–297

Yoshikawa M, Ozawa K (2007) Rb–Sr and Sm–Nd isotopic systematics of the Hayachine–Miyamori ophiolitic complex: Melt

generation process in the mantle wedge beneath an Ordovician island arc. Gondwana Res 11:234–246

Yoshikawa M, Suzuki K, Shibata T, Ozawa K (2012) Geochemical and Os isotopic characteristics of a fresh harzburgite in the Hayachine–Miyamori ophiolite: evidence for melting under influx of carbonate-rich silicate melt in an infant arc environment. J Min Petrol Sci 107:250–255